Colimitation assessment of phytoplankton growth using a resource use efficiency approach in the Bay of Seine (French-English Channel)

Serre-Fredj Léon [1, 2], Chasselin Leo [1, 3], Jolly Orianne [1, 3], Jacqueline Franck [4], Claquin Pascal [1, 2, *]

[1] Normandie Université, Université de Caen Normandie, Esplanade de la Paix, 14032, Caen, France
[2] Laboratoire Biologie des ORganismes et Ecosystèmes Aquatiques (BOREA, UMR CNRS 8067), Muséum National d'Histoire Naturelle, Sorbonne Université, Université de Caen Normandie, IRD 207, Université des Antilles. Centre de Recherches en Environnement Côtier (CREC) - Station Marine, BP49, 54, Rue du Docteur Charcot, 14530, Luc-sur-Mer, France
[3] Centre de Recherches en Environnement Côtier (CREC) - Station Marine de l'Université de Caen Normandie, BP49, 54, Rue du Docteur Charcot - 14530Ifremer LER/N, Avenue du Général de Gaulle, 14520, Port-en-Bessin, France
[4] Ifremer LER/N, Avenue du Général de Gaulle, 14520, Port-en-Bessin, France

* Corresponding author : Pascal Claquin, email address : pascal.claquin@unicaen.fr

Abstract :

Eutrophication and dystrophy are two of the main problems affecting coastal ecosystems. In the Bay of Seine, phosphorus (P) inputs from the Seine estuary have been largely reduced in the last decade, in contrast to nitrogen (N), which leads to high N/P ratio inputs. To study the effect of dystrophy, an enrichment bioassay using water sampled from the Bay of Seine was repeated 19 times over a period of 18 months with six different enrichments. After a few days, chlorophyll a (chl a), alkaline phosphatase activity (APA), transparent exopolymeric particles (TEPs), cytometric size structure, and maximum quantum yield of photosystem II were measured. The data provide strong evidence for an N & P colimitation system in the vast majority of the incubations, as only the N + P and N + P + Si enrichments supported phytoplankton growth, and Si only appeared to play a secondary role in our incubations. A N/P ratio of 16 equal to the Redfield ratio was identified as the optimum for balanced growth, as chl a was the highest and TEP and APA production was the lowest at this ratio. To fit the requirements of the colimited system, a new resource use efficiency (RUENP) calculation was developed to account for N and P colimitation instead of only one nutrient, as is usually the case. This calculation allows better representation of RUE in dystrophic conditions, as found in many highly anthropized ecosystems. The relationships between RUENP and the size structure of the phytoplankton community were explored, and a significant positive correlation between RUENP and larger cells (>2 μm) and a negative correlation with smaller cells (<2 μm) were noted, showing a better use of nutrients by larger cells. This study highlights an increase of RUENP with the phytoplankton cell size in a colimited system.

Graphical abstract
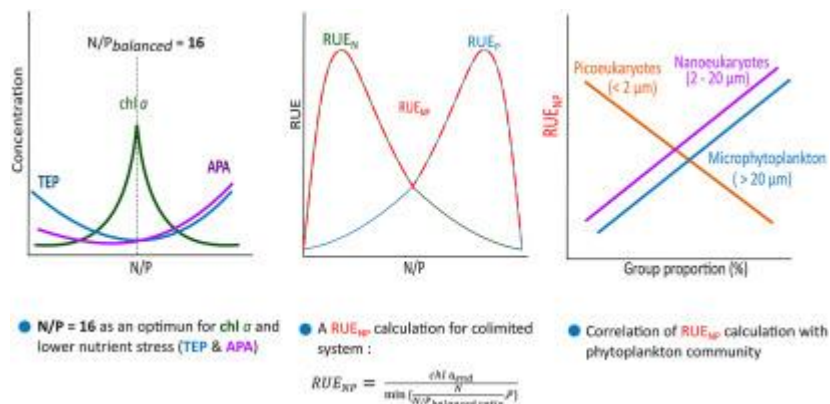
Highlights

► A colimitation system of N & P was highlighted by an enrichment experiment in the Bay of Seine. ► An optimal N/P ratio of 16 for phytoplankton growth was determined, even in dystrophic systems. ► A new resource use efficiency (RUE_{NP}) calculation was adapted to a colimited system. ► RUE_{NP} positively correlated with larger cells and negatively correlated with smaller cells.

Keywords : Eutrophication, N/P ratio, Alkaline phosphatase activity, Transparent exopolymeric particles, Flow cytometry, Ecophysiological parameters

1. Introduction

Coastal ecosystems provide important economic services, and their decline, due to multiple human pressures, could have long-term impacts (Barbier et al., 2011). The main problem facing coastal ecosystems is eutrophication (Rabalais et al., 2009), caused by excessive inputs of nutrients, usually nitrogen (N) and phosphorus (P), into the system associated with a dystrophic ratio. Phytoplankton uptake is mainly described by the Redfield ratio (N/P = 16), which regulates the nutrient system (Falkowski, 2000), but in dystrophic conditions, deviation from this paradigm can be observed at multiple scales from cellular to environmental requirements (Fraga, 2001; Geider and La Roche, 2002; Glibert and Burkholder, 2011; Ptacnik et al., 2010). However, unbalanced nutrient inputs affect phytoplankton community composition (Leruste et al., 2019; Shen et al., 2019) and growth rate (Nwankwegu et al., 2020). Thus, knowing which nutrients limit phytoplankton growth is crucial. Recently, multiple coastal ecosystems have been described as colimited systems (Chorus and Spijkerman, 2020; Conley et al., 2009; Harpole et al., 2011) with N and P as independent nutrients (Saito et al., 2008). The Bay of Seine (France) is a typical eutrophic system, and nutrients are mainly supplied by the Seine River (Aminot et al., 1998) and at a smaller scale by local rivers (Lemesle et al., 2015). In recent decades, nutrient management programmes in the Seine River have successfully reduced nutrient inputs, particularly phosphorus inputs (Aissa-Grouz et al., 2018) by improvement of domestic wastewater treatment, but N levels have nevertheless remained high (Garnier et al., 2019). This causes an abrupt change in nutrient stoichiometry with high N/P ratios measured in both the Seine estuary and the Seine River (Garnier et al., 2019; Meybeck et al., 2018).

One way to better assess the link between the phytoplankton community and nutrients is the resource use efficiency (RUE) parameter. RUE measures the supplied resources converted into biomass (Hodapp et al., 2019) and is useful to characterize the use of nutrients by phytoplankton populations. To our knowledge, only a few authors, e.g., Han et al. (2016), have broached the

82 multiple limitations of RUE, one being that RUE usually focuses on one nutrient at a time (e.g.,

83 RUE_N, RUE_P). Today, given the growing interest in colimitation systems, new insights are

84 needed to describe these nutrient regimes more precisely.

85 Enrichment bioassays are an effective way to investigate the effects of nutrient inputs on the

86 phytoplankton community (Rahav et al., 2018; Reed et al., 2016; Song et al., 2019; Van

87 Meerssche and Pinckney, 2019). Varying the composition, stoichiometry and quantity of

88 nutrients added pinpoint limitation patterns more easily (Tamminen and Andersen, 2007).

89 Repeating the bioassays throughout the year enables the identification of time-dependent

90 interactions (Xu et al., 2010).

91 To investigate the effect of nutrient enrichment on phytoplankton in the Bay of Seine, we

92 conducted repeated bioassays. After a few days of incubation, the community structure of

93 natural populations of phytoplankton was measured to assess the nutrient regime of the

94 phytoplankton community. A new approach was proposed to calculate a RUE constrained by

95 two colimiting nutrients.

96 The specific objectives of our study were to investigate the ratio of N/P consumed by the

97 phytoplankton community under unbalanced nutrient input conditions and characterize

98 physiological status and population structure responses to sudden nutrient enrichments. This

99 approach should allow us to identify the limitation system in a dynamic anthropized macrotidal

100 bay at a temperate latitude.

101

2. Materials and Methods

2.1 Measurements in the Bay of Seine

High-frequency data were monitored *in situ* over a two-year period using the SMILE (System of Measurement Integrated for Littoral and Environment) buoy. It is a moored buoy localized in the Bay of Seine (0°19'41.00"O 49°21'14.00"N) equipped with physico-chemical and biological sensors working in continuous and autonomous conditions (data available at Claquin et al., 2018).

In vivo fluorescence (Cyclops-6K, Turner Design, USA), fluorescein fluorescence units (FFU), temperature (WTW^{TM}, TetraCon, Germany) and turbidity (Seapoint Turbidity Meter, Seapoint Sensors, USA) were measured together in a multiparameter probe NKE instrument (MP7, NKE Instrumentation ®). Photosynthetically active radiation (PAR) was measured with a Satlantic sensor (Satlantics, Italy). NO_3^- was measured with an OPUS optical sensor (TriOS Mess- & Datentechnik GmbH Germany). All these parameters were measured at 20-min intervals at a depth of one metre since 2016.

PO_4^{3-} data and additional NO_3^- data come from a bimonthly sampling program (French Coastal Observation Service, https://www.somlit.fr/, Cocquempot et al., 2019) where water has been sampled near the SMILE buoy at a depth of one metre since 2013 and analysed as described in Part 2.2.1.

2.2 Enrichment experiment

Bioassays were designed to assess the impacts of enrichment on the phytoplankton assemblages and on their physiological responses. The design was modified from Ly et al. (2014) to fit our specific requirements as described in Serre-Fredj et al. (2021). The experiment was repeated 19 times over a period of 2 years on different dates (see

127 supplementary table for starting date, and Supplementary figure 2). Each incubation will be

128 referred to by its number corresponding to chronological order. Seawater was sampled at the

129 SMILE buoy site. To remove large grazers, the seawater was filtered through a 100-µm mesh

130 immediately after sampling. For the bioassays, enrichments were added to 500-ml subsamples

131 in polycarbonate bottles one hour after sampling and placed in an incubator. All bioassays

132 were incubated in a water bath incubator for 4 to 5 days (see supplementary table for specific

133 duration) under natural sunlight in a greenhouse. The water bath incubator was fuelled

134 continuously with seawater pumped directly from the sea maintaining the incubator to the

135 temperature of the bay. Seawater temperature and PAR were recorded at 5-min intervals using

136 an RBRsolo T logger and an RBR solo^3 PAR logger connected to a Li-COR LI-192

137 Underwater Quantum Sensor, respectively. Up to six types of enrichment treatments, each

138 with five replicates, were performed in the incubator for each incubation experiment: Control

139 with no addition of nutrients (C), +P (P), +N (N), +N+Si (NSI), +N+P (NP), or +N+P+Si

140 (PNSI). The enrichments applied in the bioassays were defined by the maximum value of N

141 (50 µmol.l^{-1}), P (3 µmol.l^{-1}) and Si (50 µmol.l^{-1}) measured in 2018 in the Bay of Seine by the

142 French Coastal Observation Service (SOMLIT, https://www.somlit.fr/, Cocquempot et al.,

143 2019). Two enrichments were added during the experiment: NSI was added after the 4th

144 incubation experiment, and NP was added after the 13th incubation experiment.

145

146 After 4 or 5 days, 25 ml was sampled in all bioassay bottles and homogenized before measuring

147 photosynthetic, flow cytometer and alkaline phosphatase activity (APA). TEP, nutrient and

148 chlorophyll *a* (chl *a*) concentrations were also measured at day 4 or 5. APA was included after

149 the 7th incubation and TEPs after the 9th incubation.

150 The analyses, duration, and enrichments performed are summarized in the additional table.

151

2.2.1 Measurements of inorganic nutrients (NO$_3^-$, PO$_4^{3-}$, Si(OH)$_4$)

153   Water samples were collected and filtered through a ClearLine, CA, 33 mm, 0.45 µm cellulose

154   acetate filter and immediately frozen (-20 °C), with the exception of Si(OH)$_4$, which was stored

155   at 4 °C. Analyses were conducted using a SEAL Analytical AA3 system (Aminot and Kérouel,

156   2007). The quantification limits were 0.02 µmol.l^{-1} for PO$_4^{3-}$ and 0.05 µmol.l^{-1} for NO$_3^-$, NO$_2^-$,

157   Si(OH)$_4$. The N/P ratio was calculated as NO$_3^-$/ PO$_4^{3-}$. The N/P$_{consumed}$ was calculated as (N$_{start}$-

158   N$_{end}$)/(P$_{start}$-P$_{end}$), where N$_{start}$ and P$_{start}$ represent the concentrations of N and P at the beginning

159   of the incubation (i.e., the stock of nutrients in the sampled water plus specific enrichment) and

160   N$_{end}$ and P$_{end}$ the concentrations of N and P at the end of the incubation.

161   **2.2.2 Chlorophyll-*a* measurements**

162   Water samples (250 ml) were filtered through a Whatman GF/F 47 mm, 0.7 µm glass-fibre filter

163   and immediately frozen (-20 °C) until analysis. Ten millilitres of 90% acetone (v/v) was added

164   to extract the pigment, and the samples were then left in the dark at 4 °C for 12 h. After being

165   centrifuged for 5 min at 1,700 g twice, the concentration of chl *a* in the extracts was measured

166   using a Trilogy fluorometer (Turner Designs, Sunnyvale, USA) according to the method of

167   (Strickland and Parsons, 1972). The Δchl *a* is calculated as chl *a*$_{end}$ − chl *a*$_{start}$.

168   **2.2.3 Transparent exopolymeric particles (TEP)**

169   Water samples (150-200 ml) were filtered through Millipore, 0.4 µm polycarbonate

170   membrane filters and immediately frozen (-20 °C) until analysis. Following Claquin et al.

171   (2008) adapted from Passow and Alldredge (1996), the filters were stained with a solution of

172   0.02% Alcian Blue solution (Sigma) with 0.06% acetic acid (pH: 2.5). Excess dye was removed

173   by adding water before centrifugation at 3,000 g at 19 °C for 15 min. This washing cycle was

174   repeated twice, after which 6 ml of 80% H$_2$SO$_4$ was added. After 2 h, measurements were taken

175   using a Pharmacia Biotech Ultrospec 1000 Spectrophotometer at 787 nm. Calibration was

176   performed using xanthan gum (10-700 µg) as a standard, as described in Claquin et al., (2008).

177 After being divided by the chl *a* concentration, TEP concentrations are expressed in µg Xanthan

178 eq.µg chl a^{-1}.

2.2.4 Alkaline phosphatase activity (APA)

180 The potential maximum APA per chlorophyll unit was measured according to Hrustic et

181 al. (2017). Samples (3,920 µl) were placed in a UV cuvette, and 80 µl of 500 µM 4-

182 methylumbelliferyl phosphatase (MUF-P) substrate was added. While incubating at room

183 temperature, the samples were measured at hourly intervals over a total period of 7 h.

184 Measurements were made with an RF-6000 spectrofluorophotometer (Shimadzu, Japan). APA

185 was calculated as the slope of the linear regression. Using an MUF standard curve, the results

186 are expressed in concentration units per hour divided by the concentration in chl *a* to normalize

187 by the biomass, thus obtaining $APA_{chl\ a}$ ($nM.h^{-1}.\mu g$ chl $a^{-1}.l^{-1}$).

188

2.2.5 Fluorometry to assess photosynthetic parameters

190 To measure the maximum quantum efficiency of photosystem II photochemistry (Fv/Fm), three

191 fluorimeters were used during the experiment: a Water PAM (Walz, Germany), a FRRf-ACT2

192 (Chelsea Technologies, UK) and a LabSTAF (Chelsea Technologies, UK). Oxidation of

193 quinone A (Q_A) in the samples was analysed after a 5-min period of incubation in the dark.

194 For the water-PAM measurements, the sample was excited by weak blue light (1 µmol

195 photons.$m^{-2}.s^{-1}$, 470 nm, frequency 0.6 kHz) to record the minimum fluorescence (F_0). The

196 maximum fluorescence (F_m) was obtained during a multiturnover (MT)-saturating light pulse

197 (0.6 s, 1700 µmol photons.$s^{-1}.m^{-2}$, 470 nm), which enabled reduction of the quinone A (QA)

198 pool.

199 For the ACT2-FRRF measurements, a single turnover (ST) saturation phase was delivered with

200 one hundred 1-µs flashlets at 2-µs intervals to measure F_o and maximum fluorescence (F_m) (452

201 nm) using the biophysical model of Kolber et al. (1998).

202 For the LabSTAF measurements, a single turnover (ST) saturation phase was delivered with a

203 solid 100-µs flash (450 nm) to measure minimum and maximum fluorescence, as described in

204 Boatman et al. (2019).

205   Following Genty et al. (1989), the maximum quantum efficiency of photosystem II

206 photochemistry (Fv/Fm) was calculated in Equation 1:

207

$$\frac{F_v}{F_m} = \frac{(F_m - F_0)}{F_m} \qquad (1)$$

208

209

210 A discrepancy in the Fv/Fm measurement is known between the different methods of variable

211 fluorometry used (Kromkamp and Forster, 2003). Therefore, data normalization per incubation

212 (between 0 and 1) allowed us to compare the whole set of incubations.

213

214   ***2.2.6*** **Flow cytometry**

215   Unfixed samples were analysed within one hour of sampling with a CytoSense

216 (Cytobuoy b.v., Netherland) equipped with a blue laser (488 nm, 50 mW) and a green laser (552

217 nm, 50 mW). This produces pulse shapes based on the inherent optical properties of the particle

218 when they cross the laser: sideward angle scatter (SWS), forwards scatter (FWS), red (FLR,

219 668-734 nm), orange (FLO, 601-668 nm) and yellow fluorescence (FLY, 536-601 nm). The

220 threshold was set at 16 mV to reduce data acquisition concerning nonphotosynthetic particles

221 triggered on FLR; for each sample (5 per enrichment), 380 µl was analysed with a speed of 2.0

222 µl.s^{-1}. CytoSense can analyse chains, cells, or colonies between 1 and 800 µm in diameter.

223 Microspheres of 1 µm (yellow–green fluorescent, FluoSpheres®), 1.6 µm (nonfluorescent,

224 provided by Cytobuoy) and 2 µm, 6 µm, 10 µm, and 20 µm (Fluoresbrite® YG microspheres,

225 Polyscience) were used to calibrate size recordings (daily use). To distinguish the phytoplankton

226   (Supplementary Fig. 1), five clusters were determined using the cells' optical properties and

227   attributed to *Synechococcus* spp., picoeukaryotes, nanoeukaryotes and microphytoplankton and

228   cryptophytes. The *Synechococcus* spp. cluster has the smallest FWS signal and a high orange

229   fluorescence (FLO) signal, which matches very small cells with a high concentration of

230   phycoerythrin.

231   Picoeukaryote cells are small cells (< 2 µm) and produce low FLR and FWS signals.

232   Nanoeukaryotic (2–20 µm) and microphytoplankton (> 20 µm) cells were differentiated from

233   picoeukaryotic cells using the amplitude of the FLR signal and the bead signal. Cryptophytes

234   clusters have higher FLO than *Synechococcus* due to the high concentrations of phycoerythrin

235   in their cells and an FWS equivalent to the nanoeukaryotic and microphytoplankton cells (Olson

236   et al., 1989; Thyssen et al., 2014).

237

238   *2.3 RUE calculation*

239   RUE is the amount of biomass produced per unit of supplied resource (Hodapp et al., 2019).

240   The equation proposed by Ptacnik et al. (2008) to calculate RUE (chl *a*/total P) is quite simple

241   and is the one most frequently reported in the literature (Chai et al., 2020; Filstrup et al., 2019;

242   Lehtinen et al., 2017; Yang et al., 2021) with total P as the limiting nutrient. This equation can

243   also be used with other limiting nutrients, including N (Amorim and Moura, 2021; Frank et al.,

244   2020; Olli et al., 2015; Otero et al., 2020). The dissolved organic fraction (DIN or DIP) can also

245   be used instead of the total elemental concentration (Amorim and Moura, 2021; Otero et al.,

246   2020). The need to consider stoichiometry constraints for RUE calculation has already been

247   highlighted in Frank et al. (2020).

248   Thus, to fit the colimitation hypothesis (Arrigo, 2005; Saito et al., 2008), we considered more

249   than one nutrient. The concept of colimitation and/or alternation between N and P limitation

250   according to Davidson and Howarth (2007) and Elser et al. (2007) describes how, depending

251   on the balance, N and P could incrementally limit growth one after another until one is too low

252   for uptake. The nutrient present in the smallest proportion will be the last limiting nutrient in

253   the sequence. To directly compare the concentration of both nutrients (N & P), a scale of

254   limitation has to be applied. The simplest approach largely admitted is to consider the Redfield

255   ratio as the balanced N/P ratio (Falkowski, 2000; Lips and Lips, 2008), even if it can be

256   discussed primarily in the context of coastal anthropized ecosystems (Arrigo, 2005; Chorus and

257   Spijkerman, 2020; Glibert and Burkholder, 2011). Then, N/P ratios lower than 16 are considered

258   N limited, and ratios higher than 16 are considered P limited.

259   Based on the equation of Ptacnik et al. (2008), a RUE_{NP} equation using the N/P ratio was

260   applied:

261
$$RUE_{NP} = \frac{chl\ a_{end}}{\min\{\frac{N}{N/P_{balanced\ ratio}}, P\}}$$
(2)

262
263   where chl a_{end} is the concentration at the end of the incubation, N and P concentrations

264   correspond to values of N_{start} and P_{start} of NO_3^- and PO_4^{2-}, respectively, at the beginning of

265   each incubation (i.e., the stock of nutrients in the sampled water plus specific enrichment).

266   Here, the N/P$_{balanced\ ratio}$ accounts for the 16/1 Redfield ratio (Redfield, 1958) (Equation 2).

267   The minimum function (min) makes it possible to account for the last limiting nutrient in the

268   alternating nutrient limitation system.

269   In other words, this RUE_{NP} calculation is equal to RUE_P when N/P > N/P$_{balanced}$ and to RUE_N

270   when N/P < N/P$_{balanced}$ (Figure 1). This prevents underestimation of the RUE value in

271   dystrophic cases. To illustrate the case of an extremely high N/P (e.g., 300), the RUE_N would

272   be reduced due to the excessive presence of N, even if the limiting nutrient here is P, thus

273   making the RUE_P more appropriate. The RUE_{NP} allows to cover both dystrophic cases.

274

275   *2.4 Statistical analysis*

276   All analyses were conducted in R (R-project, CRAN) version 3.6.1. To better display

277   variations due to the enrichment data used for the heatmap (e.g., Figures 2, 3, 4 and 5) are all

278   normalized between 0 and 1 per incubation, such that the maximum value of the parameter in

279   each incubation is 1 and the minimum is 0. As the incubation data did not follow a normal

280   distribution, a Kruskal–Wallis test was performed using the "stats" package, and a Conover-

281   Iman pairwise test was performed using the "conover.test" package. Only significant tests

282   with a p value < 0.05 were accepted. PCA and hierarchical cluster analyses were performed

283   using the "FacoMineR" (Lê et al., 2008) and "factoextra" (Kassambara, 2017) packages. The

284   last six incubations were included in the multivariate analysis (13th to 19th incubations) to

285   include all types of enrichment. The number of clusters for the k-means clustering analysis

286   was chosen using silhouette analysis.

287

3. Results and discussion

3.1 Environmental parameter in the Bay

Figure 2 shows two years of high-frequency data in the Bay of Seine measured by the SMILE buoy. The temperature ranged from 8.1 °C to 22.5 °C, and a maximum fluorescence value of 481 FFU was recorded on the date of the 19th sampling (12/10/2020). Fluorescence followed standard patterns (Napoléon et al., 2012) with higher values in spring and summer, while late blooms could occur in autumn, as shown by the 9th incubation event, which represented the highest value in 2019 (170 FFU) (Fig. 2. A). The two inorganic nutrients (NO_3^- and PO_4^{3-}) displayed the opposite pattern of temperature, i.e., replenished in winter and depleted in summer due to nutrient consumption. NO_3^- ranged from the limit of detection 0.01 to 69.27 µmol.l^{-1} (Fig. 2. C) and PO_4^{3-} ranged from the limit of detection 0.02 to 1.01 µmol.l^{-1} (Fig. 2. D). A wide range of variation is depicted by the incubation that may affect phytoplankton community and response even if a majority (60%) are gathered within the high production zone from May to October. Out of this time period, light intensity may be more limiting than nutrients, as displayed by replenishing nutrient levels (Napoléon et al., 2014, 2012). Moreover, some extreme events are present, such as the 9th or 19th incubation, which both account for massive blooms, as flagged by the fluorescence increase.

3.2 Phytoplankton growth link with nutrient balance

Figure 3 presents the chl a_{start} concentration measured at the beginning of the incubation and final concentration for each enrichment for all bioassays and all enrichments. The results showed that in 17 incubations out of 19, NPSi enrichment presented the highest chl a concentration (Fig. 3. A). Both NP and PNSI enrichments showed high chl a concentrations with averages of 20.9 µg chl a^{-1}.l^{-1} and 24.5 µg chl a^{-1}.l^{-1}, respectively, and differed

314   significantly from other treatments (Kruskal–Wallis: $\chi^2 = 29.26$, $p_{value} = 5.4 \times 10^{-5}$; followed by

315   Conover test, $p_{value} = 3.6 \times 10^{-4}$, 8.7×10^{-4}). This result highlights evidence for colimitation of N

316   and P, as NP and PNSi enrichment displays maximum growth. The lack of a significant

317   difference between NP and NPSI indicates the secondary role of Si. Incubations 3, 5, 10, 11

318   and 12 display little to no growth regardless of the enrichment, indicating other limitations. As

319   underlined in Section 3.1, this could be due to suboptimal temperature and light conditions for

320   phytoplankton growth.

321   When compared to the log of the N/P$_{consumed}$ ratio during the incubation, the chl *a* distribution

322   showed a peak. The weighted mean of the 9th percentile of the chl *a* distribution

323   corresponding to the N/P ratio peak value was 16.01, which corresponds to the Redfield ratio

324   (Fig. 3. B). This optimum growth of the phytoplankton community at a N/P Redfield is not

325   surprising (Klausmeier et al., 2004) and is in agreement with the results of a recent study by

326   Zheng et al. (2020), who showed a consumed N/P ratio of 16 in the overenriched Bohai Sea in

327   China. However, a discrepancy from this ratio could have been expected under dystrophic

328   input (Geider and La Roche, 2002; Glibert and Burkholder, 2011).

329

330   3.3 Limitation assessment by physiological parameter

331   3.3.1 APA - TEP

332   TEP$_{chl\ a}$ displayed a nonhomogenous distribution in the "high-TEP$_{chl\ a}$ concentration" groups,

333   with C, P, N, and NSi enrichments, and in the "low-TEP$_{chl\ a}$ concentration" group, with D$_0$, NP

334   and PNSi enrichments (Kruskal–Wallis: $\chi^2 = 36.5$, $p_{value} = 2.2 \times 10^{-6}$; followed by the Conover

335   test: mean p value= 5.9×10^{-4}) (Fig. 4. A). When TEP$_{chl\ a}$ concentrations were compared to

336   log(N/P), the minimum value of TEP$_{chl\ a}$ identified by the regression function corresponded to

337   an N/P ratio of 26.42, diverting from this minimum the function rise up at low and high N/P

338   values (Fig. 4. B).

339   The same approach was applied to the $APA_{chl\ a}$ dataset. Data analysis of $APA_{chl\ a}$ (Kruskal–

340   Wallis: χ^2 = 16.78, p_{value} = $1.0x10^{-2}$; followed by the Conover test: mean p_{value}= $3.0x10^{-4}$)

341   highlighted two groups: "high $APA_{chl\ a}$" corresponding to C, N, NSi enrichments and "low

342    $APA_{chl\ a}$" corresponding to D0, P, NP and PNSi enrichments (Fig. 4. C). When compared to the

343   log(N/P ratio), the minimum value of $APA_{chl\ a}$ of the regression function, which resembled a

344   parabola, corresponded to an N/P ratio of 16.26, diverting from this minimum, the function rose

345   faster at a high N/P ratio than at a low N/P ratio (Fig. 4. D).

346   As APA is produced by phytoplankton and prokaryotes to convert organic P into accessible

347   inorganic P (Falkowski and Raven, 1998; Lin et al., 2016), it is used as an indicator of P

348   limitation (Serre-Fredj et al., 2021; Tanaka et al., 2006). Enrichment without P addition (*e.g.,*

349   C, N and NSI) displays a higher APA value, which is in agreement with Elser and Kimmel

350   (1986). Surprisingly, no difference was found between the D0 value of APA and the APA

351   measured for P, NP and PNSI enrichments. This result may contradict a potential P limitation.

352   Even after sustaining P, APA levels may remain high due to internal storage of the alkaline

353   phosphatase enzyme (Litchman and Nguyen, 2008).

354   When compared to the N/P ratio values, the increase in APA at a low N/P (i.e., N-limited) ratio

355   can be disconcerting but has already been reported in the literature (Kuenzler and Perras, 1965).

356   APA production can be triggered by N limitation (Kuenzler and Perras, 1965) or change as a

357   function of the community structure (Lin et al., 2015; Yuan et al., 2017). Our results show that

358   a high level of APA may reveal an unbalanced N/P ratio rather than being an absolute indicator

359   of P limitation.

360   TEPs are indicators of carbon excretion (Claquin et al., 2008; Klein et al., 2011) and could be

361   used as a metabolic overflow of carbon under nutrient limitation. Although Claquin et al. (2008)

showed that TEPs are also produced during balanced growth, in the literature, an increase in TEP production has been reported to be associated with N limitation (Beauvais et al., 2003; Corzo et al., 2000; Deng et al., 2016), with P limitation (Pandey and Pandey, 2015) and with variations in the N/P ratio (Engel et al., 2015; Mari et al., 2005). Our results are consistent with these hypotheses, suggesting that digressing from a balanced N/P ratio (i.e., N/P = 16) increases TEP production. Only the addition of at least N and P appeared to reduce TEP production. All other partial enrichments (C, N, P and NSi) increased TEP, which is consistent with the nutrient limitations of the phytoplankton community we identified in this study.

Some exceptions to this general trend were observed. During the 10th (16/09/2019) incubation, a high concentration of TEPs was associated with an N/P ratio near the Redfield ratio. High TEP concentrations are frequently observed at the end of summer due to increased phytoplankton biomass (Parinos et al., 2017; Serre-Fredj et al., 2021), and Claquin et al. (2008) showed that under balanced growth, an increase in temperature was associated with an increase in TEP production by diatoms. The high value of TEPs in the 10th incubation could be caused by a high initial stock of TEPs in the water sample because of a bloom of *Lepidodinium chlorophorum* (Serre-Fredj et al., 2021)*,* a huge TEP producer (Claquin et al., 2008), which occurred two weeks before (Serre-Fredj et al., 2021).

The physiological response of the phytoplankton community, illustrated here by APA and TEPs, supports the hypothesis of the optimum balance of the N/P ratio of approximately 16, as the addition of balanced nutrients reduces the values of both physiological indicators. In addition, the dynamics of both indicators (APA and TEPs) confirmed the secondary role played by Si inputs in the bioassays.

3.3.2 Maximun quantum efficiency of photosystem II (Fv/Fm)

387 The Fv/Fm in the bioassays ranged from 0.19 to 0.62. These values display intraincubation

388 patterns that distinguish the two groups. In 9 out of 13 incubations (70%), complete enrichment

389 showed the highest values among incubation, resulting in PNSI being a separate group

390 (Kruskal–Wallis: $\chi^2 = 20.6$, $_{p\ value} = 3.8x10^{-4}$, Conover: mean = $2.2x10^{-3}$). In all other cases, D0

391 displayed the maximum value but was not significantly different from the other enrichments

392 (Fig. 5. A). In addition to influencing the biomass or physiology of the bulk community,

393 enrichment with a different stoichiometry affects the structure (Piehler et al., 2004), growth

394 (Watanabe et al., 2017) and photosynthesis (Song et al., 2019) of the phytoplankton community

395 (Serre-Fredj et al., 2021). A decrease in the maximum quantum yield of photosystem II (Fv/Fm)

396 has been associated with many factors, including temperature (Zhang et al., 2012), parasite

397 attacks (Park et al., 2002) and particularly nutrient limitation (Behrenfeld et al., 2004; Claquin

398 et al., 2010). Here, the addition of both N and P increased this physiological indicator status in

399 most cases, which is in accordance with the APA and TEP dynamics.

400

401 3.5 Phytoplankton community

402 The concentration of *Synechococcus* dropped in most incubations regardless of the enrichment.

403 NP enrichment was still identified as a separate group (Kruskal–Wallis: $\chi^2 = 16.8$, $p_{value} =$

404 $7.8x10^{-3}$, Conover: mean = $4.4x10^{-3}$) due to the high concentration of *Synechococcus* measured

405 in the final (from the 15th -16/06/2020 to the 19th – 12/10/2020) incubations, with a maximum

406 of $8.9x10^4$ cells.cm^{-3} in the 19th incubation (Fig. 5. B).

407 The concentration of picoeukaryotes appeared to be affected over time, and PNSI enrichment

408 was identified as a separate cluster due to the high concentration of this population (Kruskal–

409 Wallis: $\chi^2 = 22.3$, $p_{value} = 4.0x10^{-4}$, Conover: mean = $5.2x10^{-4}$), as the maximum value was

410 $1.7x10^5$ cells.cm^{-3} in the 4th incubation, PNSI enrichment (Fig. 5. C). Nanoeukaryotes followed

411 exactly the same pattern as picoeukaryotes, with PNSI enrichment identified as a separate

412   population (Kruskal–Wallis: χ^2 = 25.2, p_{value} = 1.3×10^{-4}, Conover: mean = 3.6×10^{-3}). The pattern

413   of cryptophytes was less certain, depending on the incubation, the maximum value could be

414   reached by all enrichments, nonetheless, NP was highlighted as a separate group (Kruskal–

415   Wallis: χ^2 = 20.0, p_{value} = 9.3×10^{-4}, Conover: mean NP= 4.4×10^{-3}, mean PNSI= 2.3×10^{-3}), as the

416   *Synechococcus*-normalized value of cryptophytes was high in the final incubations (15th to 19th)

417   (Fig. 5. C).

418   The concentration of microphytoplankton followed a pattern similar to that of the

419   nanoeukaryotes, and PNSI was again identified as a separate group (Kruskal–Wallis: χ^2 =

420   25.0, p_{value} = 1.1×10^{-4}, Conover: mean = 5.0×10^{-4}) (Fig. 5. D). The size structure of the

421   phytoplankton population must be taken into account, as PNSi enrichment allowed maximum

422   growth of the picoeukaryotes, nanoeukaryotes and microphytoplankton in most of the

423   incubations. With the exception of the 15th and 16th incubations, *Synechococcus* seemed

424   unable to grow in these conditions. This result could be a bias caused by the closed system,

425   which could increase predatory pressure associated with a higher death rate of this taxon

426   (Agawin et al., 2000). Another possible hypothesis is that larger cells, such as diatoms,

427   compete more successfully with high enrichment pulses than *Synechococcus* and cryptophytes

428   (Van Meerssche and Pinckney, 2019).

429

430   3.6 Multivariate analysis and overall trend

431   Figure 6 shows the multivariate results of the last six incubations (see Section 2.4 for

432   precision on the choice). The two dimensions of the PCA explained up to 66.3% of the total

433   variance and are summarized by a few statements (Fig. 6. A): The chl *a* concentration was

434   positively correlated with the concentration of picoeukaryotes, nanoeukaryotes and

435   microphytoplankton (i). APA, TEPs, RUE and the proportion of picoeukaryotes were

436   positively intercorrelated and negatively correlated with chl *a* (ii). The proportions of

437   microphytoplankton and nanoeukaryotes were opposite but not correlated with any of the

438   other parameters (iii). This pinpoints a change in the phytoplankton community linked with

439   nutrient enrichment and the N/P ratio, as limitations seem to favour populations with higher

440   proportions of picoeukaryotes, while replete and balanced conditions favour nanoeukaryote

441   and microphytoplankton populations.

442   Cluster analysis identified three groups (Fig. 6. B & C): The first group was only composed of

443   C, N, P and NSi enrichments, the second group was composed of NP and PNSi enrichments,

444   with the exception of P enrichment in the 13th incubation, and the last group was composed of

445   all the enrichments in the 19th incubation already highlighted as an extreme event of massive

446   bloom.

447

448   3.7 Link between RUE and the phytoplankton community

449   RUE is usually calculated as chl a or the primary production divided by N or P (Filstrup et al.,

450   2014; Olli et al., 2015; Ptacnik et al., 2008), but our result highlights the fact that N and P

451   colimitation and the stoichiometry constraint summarized in the N/P ratio are important

452   regarding the RUE (Frank et al., 2020). Moreover, both the increase in chl a and phytoplankton

453   physiological parameters (TEPs and APA) suggest that the Redfield ratio is optimum for

454   community uptake. In our case, only accounting for nutrients would have involved loss of

455   information and an important skew due to a colimited system. The equation of RUE_{NP} we use

456   accounts for both the quantity of nutrients—by directly using the concentration—and the

457   balance of nutrients—by prioritizing the limiting nutrient. This kind of model, which resembles

458   multiple resource use efficiency (mRUE), could be more effective and help understand both

459   resource use efficiency and ecosystem production (Han et al., 2016).

460   The relation between RUE_{NP} and the cytometric size structure of the phytoplankton population

461   (Figure 7) pointed out two trends: the proportion of picoeucaryotes was negatively correlated

462   ($r^2 = 0.13$, F = 13.7, $p_{value}= 3.8\times10^{-4}$) with RUE_{NP} (Fig. 7. A), while both proportions of the

463   largest phytoplankton classes, nanoeukaryotes ($r^2 = 0.13$, F = 11.3, $p_{value}= 1.2\times10^{-3}$) and

464   microphytoplankton ($r^2 = 0.27$, F = 29.2, $p_{value}= 6.8\times10^{-7}$), were positively correlated with

465   RUE_{NP} (Fig. 7. B & C).

466   Concerning the RUE, we provide evidence for a relationship between size-structure groups and

467   RUE_{NP}, where smaller classes of phytoplankton (< 2 µm) are negatively correlated and higher

468   classes (> 2 µm) are positively correlated. RUE has been positively linked with diversity (Chai

469   et al., 2020; Otero et al., 2020; Paczkowska et al., 2019), but to our knowledge, no information

470   linking size structure with RUE has been reported to date. The use of size class instead of classic

471   diversity may be more powerful, as cell size largely controls the efficiency of the nutrient uptake

472   rate (Zaoli et al., 2019).

473   Furthermore, the coastal environment with rich inputs found in the Bay of Seine creates a

474   dynamic nutrient system with nutrient pulses (e.g., inputs from local rivers). Larger cells can

475   have 200,000 and 20,000 times more biovolume and carbon/cell volume, respectively, than

476   smaller cells (Harrison et al., 2015), and larger cells may grow better and especially have

477   more storage capacity, which helps them maintain a highly dynamic system (Malerba et al.,

478   2018). Their storage capacity and luxury uptake of carbon may also render night-time nutrient

479   uptake possible (Gardner-Dale et al., 2017), and larger cells may have even better carbon

480   acquisition (Malerba et al., 2021). These characteristics balance the lower nutrient uptake of

481   picoeukaryotes (Hein et al., 1995; Probyn and Painting, 1985). In this study, colimitation was

482   observed in the incubations. The balance of a Redfield $N/P_{consumed}$ ratio has been highlighted

483   as optimum for increased biomass of the phytoplankton population, and both APA and TEPs

484   pointed to the same ratio needed to reduce nutrient stress. No other single resource use

485   efficiency can fulfil these needs compared to RUE_{NP}. This study provides evidence that using

486   stoichiometry (Frank et al., 2020) and multiple resources in resource use efficiency (*m*RUE)

487   (Han et al., 2016) can advance our understanding of resource use efficiency and ecosystem

488   production. Furthermore, the relationship highlighted between RUE and size community

489   structure should help to understand and establish ecosystem trajectories as a function of

490   management programs to reduce nutrient inputs in coastal ecosystems.

4. Conclusion

This study investigated the effect of nutrient composition on the growth, population structure, and physiological status of phytoplankton using bioassays. The N/P ratio was shown to be the main driver of the phytoplankton community composition and physiology in the Bay of Seine, even if both a balanced (e.g., N/P = 16) and a nutrient stock are needed to maintain phytoplankton growth. The nutrient balance of the inputs affects both the physiological and population structure of phytoplankton. To fulfil our requirements, we proposed a new RUE_{NP} approach, which showed a correlation with the size structure of the phytoplankton community.

Acknowledgements

512 Agawin, N.S.R., Duarte, C.M., Agustí, S., 2000. Nutrient and temperature control of the
513   contribution of picoplankton to phytoplankton biomass and production. Limnol.
514   Oceanogr. 45, 591–600. https://doi.org/10.4319/lo.2000.45.3.0591
515 Aissa-Grouz, N., Garnier, J., Billen, G., 2018. Long trend reduction of phosphorus wastewater
516   loading in the Seine: determination of phosphorus speciation and sorption for
517   modeling algal growth. Environ. Sci. Pollut. Res. 25, 23515–23528.
518   https://doi.org/10.1007/s11356-016-7555-7
519 Aminot, A., Guillaud, J.-F., Andrieux-Loyer, F., Kérouel, R., Cann, P., 1998. Nutrients and
520   phytoplanktonic growth in the Bay of Seine, France. Oceanol. Acta 6, 923–935.
521 Aminot, A., Kérouel, R., 2007. Dosage automatique des nutriments dans les eaux marines:
522   méthodes en flux continu. Editions Quae.
523 Amorim, C.A., Moura, A. do N., 2021. Ecological impacts of freshwater algal blooms on
524   water quality, plankton biodiversity, structure, and ecosystem functioning. Sci. Total
525   Environ. 758, 143605. https://doi.org/10.1016/j.scitotenv.2020.143605
526 Arrigo, K.R., 2005. Marine microorganisms and global nutrient cycles. Nature 437, 349–355.
527   https://doi.org/10.1038/nature04159
528 Barbier, E.B., Hacker, S.D., Kennedy, C., Koch, E.W., Stier, A.C., Silliman, B.R., 2011. The
529   value of estuarine and coastal ecosystem services. Ecol. Monogr. 81, 169–193.
530   https://doi.org/10.1890/10-1510.1
531 Beauvais, S., Pedrotti, M.L., Villa, E., Lemée, R., 2003. Transparent exopolymer particle
532   (TEP) dynamics in relation to trophic and hydrological conditions in the NW
533   Mediterranean Sea. Mar. Ecol. Prog. Ser. 262, 97–109.
534   https://doi.org/10.3354/meps262097
535 Behrenfeld, M.J., Prasil, O., Babin, M., Bruyant, F., 2004. In Search of a Physiological Basis
536   for Covariations in Light-Limited and Light-Saturated Photosynthesis1. J. Phycol. 40,
537   4–25. https://doi.org/10.1046/j.1529-8817.2004.03083.x
538 Boatman, T.G., Geider, R.J., Oxborough, K., 2019. Improving the Accuracy of Single
539   Turnover Active Fluorometry (STAF) for the Estimation of Phytoplankton Primary
540   Productivity (PhytoPP). Front. Mar. Sci. 6. https://doi.org/10.3389/fmars.2019.00319
541 Chai, Z.Y., Wang, H., Deng, Y., Hu, Z., Zhong Tang, Y., 2020. Harmful algal blooms
542   significantly reduce the resource use efficiency in a coastal plankton community. Sci.
543   Total Environ. 704, 135381. https://doi.org/10.1016/j.scitotenv.2019.135381
544 Chorus, I., Spijkerman, E., 2020. What Colin Reynolds could tell us about nutrient limitation,
545   N:P ratios and eutrophication control. Hydrobiologia. https://doi.org/10.1007/s10750-
546   020-04377-w
547 Claquin, P., Jacqueline, F., Repecaud, M., Riou, P., 2018. MAREL SMILE buoy data and
548   metadata from coriolis Data Centre. https://doi.org/10.17882/53689
549 Claquin, P., NÍ Longphuirt, S., Fouillaron, P., Huonnic, P., Ragueneau, O., Klein, C.,
550   Leynaert, A., 2010. Effects of simulated benthic fluxes on phytoplankton dynamic and
551   photosynthetic parameters in a mesocosm experiment (Bay of Brest, France). Estuar.
552   Coast. Shelf Sci. 86, 93–101. https://doi.org/10.1016/j.ecss.2009.10.017
553 Claquin, P., Probert, I., Lefebvre, S., Veron, B., 2008. Effects of temperature on
554   photosynthetic parameters and TEP production in eight species of marine microalgae.
555   Aquat. Microb. Ecol. 51, 1–11. https://doi.org/10.3354/ame01187
556 Cocquempot, L., Delacourt, C., Paillet, J., Riou, P., Aucan, J., Castelle, B., Charria, G.,
557   Claudet, J., Conan, P., Coppola, L., Hocdé, R., Planes, S., Raimbault, P., Savoye, N.,
558   Testut, L., Vuillemin, R., 2019. Coastal Ocean and Nearshore Observation: A French
559   Case Study. Front. Mar. Sci. 6:324. https://doi.org/10.3389/fmars.2019.00324

Conley, D.J., Paerl, H.W., Howarth, R.W., Boesch, D.F., Seitzinger, S.P., Havens, K.E., Lancelot, C., Likens, G.E., 2009. Controlling Eutrophication: Nitrogen and Phosphorus. Science 323, 1014–1015. https://doi.org/10.1126/science.1167755

Corzo, A., Morillo, J.A., Rodríguez, S., 2000. Production of transparent exopolymer particles (TEP) in cultures of *Chaetoceros calcitrans* under nitrogen limitation. Aquat. Microb. Ecol. 23, 63–72. https://doi.org/10.3354/ame023063

Davidson, E.A., Howarth, R.W., 2007. Nutrients in synergy. Nature 449, 1000–1001. https://doi.org/10.1038/4491000a

Deng, W., Cruz, B.N., Neuer, S., 2016. Effects of nutrient limitation on cell growth, TEP production and aggregate formation of marine Synechococcus. Aquat. Microb. Ecol. 78, 39–49. https://doi.org/10.3354/ame01803

Elser, J.J., Bracken, M.E.S., Cleland, E.E., Gruner, D.S., Harpole, W.S., Hillebrand, H., Ngai, J.T., Seabloom, E.W., Shurin, J.B., Smith, J.E., 2007. Global analysis of nitrogen and phosphorus limitation of primary producers in freshwater, marine and terrestrial ecosystems. Ecol. Lett. 10, 1135–1142. https://doi.org/10.1111/j.1461-0248.2007.01113.x

Elser, J.J., Kimmel, B.L., 1986. Alteration of phytoplankton phosphorus status during enrichment experiments: implications for interpreting nutrient enrichment bioassay results. Hydrobiologia 133, 217–222. https://doi.org/10.1007/BF00005593

Engel, A., Borchard, C., Loginova, A.N., Meyer, J., Hauss, H., Kiko, R., 2015. Effects of varied nitrate and phosphate supply on polysaccharidic and proteinaceous gel particles production during tropical phytoplankton bloom experiments. Biogeosciences BG 12, 5647–5665. https://doi.org/10.5194/bg-12-5647-2015.

Falkowski, P., 2000. Rationalizing elemental ratios in unicellular algae. J. Phycol., 36, pp. 3-6, https://doi.org/10.1046/j.1529-8817.2000.99161.x

Falkowski, P.G., Raven, J.A., 1998. Review of Aquatic Photosynthesis. New Phytol. 140, 597–598.

Filstrup, C.T., Hillebrand, H., Heathcote, A.J., Harpole, W.S., Downing, J.A., 2014. Cyanobacteria dominance influences resource use efficiency and community turnover in phytoplankton and zooplankton communities. Ecol. Lett. 17, 464–474. https://doi.org/10.1111/ele.12246

Filstrup, C.T., King, K.B.S., McCullough, I.M., 2019. Evenness effects mask richness effects on ecosystem functioning at macro-scales in lakes. Ecol. Lett. 22, 2120–2129. https://doi.org/10.1111/ele.13407

Fraga, F., 2001. Phytoplanktonic biomass synthesis: application to deviations from Redfield stoichiometry. Sci. Mar. 65, 153–169. https://doi.org/10.3989/scimar.2001.65s2153

Frank, F., Danger, M., Hillebrand, H., Striebel, M., 2020. Stoichiometric constraints on phytoplankton resource use efficiency in monocultures and mixtures. Limnol. Oceanogr. 65, 1734–1746. https://doi.org/10.1002/lno.11415

Gardner-Dale, D.A., Bradley, I.M., Guest, J.S., 2017. Influence of solids residence time and carbon storage on nitrogen and phosphorus recovery by microalgae across diel cycles. Water Res. 121, 231–239. https://doi.org/10.1016/j.watres.2017.05.033

Garnier, J., Riou, P., Le Gendre, R., Ramarson, A., Billen, G., Cugier, P., Schapira, M., Théry, S., Thieu, V., Ménesguen, A., 2019. Managing the Agri-Food System of Watersheds to Combat Coastal Eutrophication: A Land-to-Sea Modelling Approach to the French Coastal English Channel. Geosciences 9, 441. https://doi.org/10.3390/geosciences9100441

Geider, R., La Roche, J., 2002. Redfield revisited: variability of C:N:P in marine microalgae and its biochemical basis. Eur. J. Phycol. 37, 1–17. https://doi.org/10.1017/S0967026201003456

610 Genty, B., Briantais, J.-M., Baker, N.R., 1989. The relationship between the quantum yield of
611   photosynthetic electron transport and quenching of chlorophyll fluorescence. Biochim.
612   Biophys. Acta BBA - Gen. Subj. 990, 87–92. https://doi.org/10.1016/S0304-
613   4165(89)80016-9

614 Glibert, P.M., Burkholder, J.M., 2011. Harmful algal blooms and eutrophication: "strategies"
615   for nutrient uptake and growth outside the Redfield comfort zone. Chin. J. Oceanol.
616   Limnol. 29, 724–738. https://doi.org/10.1007/s00343-011-0502-z

617 Han, J., Chen, J., Miao, Y., Wan, S., 2016. Multiple Resource Use Efficiency (m RUE): A
618   New Concept for Ecosystem Production. Sci. Rep. 6, 37453.
619   https://doi.org/10.1038/srep37453

620 Harpole, W.S., Ngai, J.T., Cleland, E.E., Seabloom, E.W., Borer, E.T., Bracken, M.E.S., Elser,
621   J.J., Gruner, D.S., Hillebrand, H., Shurin, J.B., Smith, J.E., 2011. Nutrient co-
622   limitation of primary producer communities. Ecol. Lett. 14, 852–862.
623   https://doi.org/10.1111/j.1461-0248.2011.01651.x

624 Harrison, P.J., Zingone, A., Mickelson, M.J., Lehtinen, S., Ramaiah, N., Kraberg, A.C., Sun,
625   J., McQuatters-Gollop, A., Jakobsen, H.H., 2015. Cell volumes of marine
626   phytoplankton from globally distributed coastal data sets. Estuar. Coast. Shelf Sci.,
627   Special Issue: Global Patterns of Phytoplankton Dynamics in Coastal Ecosystems 162,
628   130–142. https://doi.org/10.1016/j.ecss.2015.05.026

629 Hein, Pedersen, F, M., Sand-Jensen, 1995. Size-dependent nitrogen uptake in micro- and
630   macroalgae. Mar. Ecol. Prog. Ser. 118, 247–253. https://doi.org/10.3354/meps118247

631 Hodapp, D., Hillebrand, H., Striebel, M., 2019. "Unifying" the Concept of Resource Use
632   Efficiency in Ecology. Front. Ecol. Evol.
633   6:233.https://doi.org/10.3389/fevo.2018.00233

634 Hrustic, E., Lignell, R., Riebesell, U., Thingstad, T.F., 2017. Exploring the distance between
635   nitrogen and phosphorus limitation in mesotrophic surface waters using a sensitive
636   bioassay. Biogeosciences 14, 379–387. https://doi.org/10.5194/bg-14-379-2017

637 Kassambara, A., 2017. Practical Guide To Principal Component Methods in R: PCA, M(CA),
638   FAMD, MFA, HCPC, factoextra. STHDA.

639 Klausmeier, C.A., Litchman, E., Daufresne, T., Levin, S.A., 2004. Optimal nitrogen-to-
640   phosphorus stoichiometry of phytoplankton. Nature 429, 171–174.
641   https://doi.org/10.1038/nature02454

642 Klein, C., Claquin, P., Pannard, A., Napoléon, C., Roy, B.L., Véron, B., 2011. Dynamics of
643   soluble extracellular polymeric -substances and transparent exopolymer particle pools
644   in coastal ecosystems. Mar. Ecol. Prog. Ser. 427, 13–27.
645   https://doi.org/10.3354/meps09049

646 Kolber, Z.S., Prášil, O., Falkowski, P.G., 1998. Measurements of variable chlorophyll
647   fluorescence using fast repetition rate techniques: defining methodology and
648   experimental protocols. Biochim. Biophys. Acta BBA - Bioenerg. 1367, 88–106.
649   https://doi.org/10.1016/S0005-2728(98)00135-2

650 Kromkamp, J.C., Forster, R.M., 2003. The use of variable fluorescence measurements in
651   aquatic ecosystems: differences between multiple and single turnover measuring
652   protocols and suggested terminology. Eur. J. Phycol. 38, 103–112.
653   https://doi.org/10.1080/0967026031000094094

654 Kuenzler, E.J., Perras, J.P., 1965. Phosphatases of marine algae. Biol. Bull. 128, 271–284.
655   https://doi.org/10.2307/1539555

656 Lê, S., Josse, J., Husson, F., 2008. FactoMineR: An R package for multivariate analysis. J.
657   Stat. Softw. 25, 1–18.

Lehtinen, S., Tamminen, T., Ptacnik, R., Andersen, T., 2017. Phytoplankton species richness, evenness, and production in relation to nutrient availability and imbalance. Limnol. Oceanogr. 62, 1393–1408. https://doi.org/10.1002/lno.10506

Lemesle, S., Mussio, I., Rusig, A.-M., Menet-Nédélec, F., Claquin, P., 2015. Impact of seaweed beachings on dynamics of δ15N isotopic signatures in marine macroalgae. Mar. Pollut. Bull. 97, 241–254. https://doi.org/10.1016/j.marpolbul.2015.06.010

Leruste, A., Pasqualini, V., Garrido, M., Malet, N., De Wit, R., Bec, B., 2019. Physiological and behavioral responses of phytoplankton communities to nutrient availability in a disturbed Mediterranean coastal lagoon. Estuar. Coast. Shelf Sci. 219, 176–188. https://doi.org/10.1016/j.ecss.2019.02.014

Lin, S., Litaker, R.W., Sunda, W.G., 2016. Phosphorus physiological ecology and molecular mechanisms in marine phytoplankton. J. Phycol. 52, 10–36. https://doi.org/10.1111/jpy.12365

Lin, X., Wang, L., Shi, X., Lin, S., 2015. Rapidly diverging evolution of an atypical alkaline phosphatase (PhoAaty) in marine phytoplankton: insights from dinoflagellate alkaline phosphatases. Front. Microbiol. 6. https://doi.org/10.3389/fmicb.2015.00868

Lips, I., Lips, U., 2008. Abiotic factors influencing cyanobacterial bloom development in the Gulf of Finland (Baltic Sea). Hydrobiologia 614, 133–140. https://doi.org/10.1007/s10750-008-9449-2

Litchman, E., Nguyen, B.L.V., 2008. Alkaline Phosphatase Activity as a Function of Internal Phosphorus Concentration in Freshwater Phytoplankton1. J. Phycol. 44, 1379–1383. https://doi.org/10.1111/j.1529-8817.2008.00598.x

Ly, J., Philippart, C.J.M., Kromkamp, J.C., 2014. Phosphorus limitation during a phytoplankton spring bloom in the western Dutch Wadden Sea. J. Sea Res. 88, 109–120. https://doi.org/10.1016/j.seares.2013.12.010

Malerba, M.E., Marshall, D.J., Palacios, M.M., Raven, J.A., Beardall, J., 2021. Cell size influences inorganic carbon acquisition in artificially selected phytoplankton. New Phytol. 229, 2647–2659. https://doi.org/10.1111/nph.17068

Malerba, M.E., Palacios, M.M., Marshall, D.J., 2018. Do larger individuals cope with resource fluctuations better? An artificial selection approach. Proc. R. Soc. B Biol. Sci. 285, 20181347. https://doi.org/10.1098/rspb.2018.1347

Mari, X., Rassoulzadegan, F., Brussaard, C.P.D., Wassmann, P., 2005. Dynamics of transparent exopolymeric particles (TEP) production by Phaeocystis globosa under N- or P-limitation: a controlling factor of the retention/export balance. Harmful Algae, Bloom Dynamics and Biological Control of Phaeocystis: a HAB Species in European Coastal Waters 4, 895–914. https://doi.org/10.1016/j.hal.2004.12.014

Meybeck, M., Lestel, L., Carré, C., Bouleau, G., Garnier, J., Mouchel, J.M., 2018. Trajectories of river chemical quality issues over the Longue Durée: the Seine River (1900S–2010). Environ. Sci. Pollut. Res. 25, 23468–23484. https://doi.org/10.1007/s11356-016-7124-0

Napoléon, C., Fiant, L., Raimbault, V., Riou, P., Claquin, P., 2014. Dynamics of phytoplankton diversity structure and primary productivity in the English Channel. Mar. Ecol. Prog. Ser. 505, 49–64. https://doi.org/10.3354/meps10772

Napoléon, C., Raimbault, V., Fiant, L., Riou, P., Lefebvre, S., Lampert, L., Claquin, P., 2012. Spatiotemporal dynamics of physicochemical and photosynthetic parameters in the central English Channel. J. Sea Res. 69, 43–52. https://doi.org/10.1016/j.seares.2012.01.005

Nwankwegu, A.S., Li, Y., Huang, Y., Wei, J., Norgbey, E., Lai, Q., Sarpong, L., Wang, K., Ji, D., Yang, Z., Paerl, H.W., 2020. Nutrient addition bioassay and phytoplankton community structure monitored during autumn in Xiangxi Bay of Three Gorges

Reservoir, China. Chemosphere 247, 125960.
https://doi.org/10.1016/j.chemosphere.2020.125960

Olli, K., Klais, R., Tamminen, T., 2015. Rehabilitating the cyanobacteria – niche partitioning, resource use efficiency and phytoplankton community structure during diazotrophic cyanobacterial blooms. J. Ecol. 103, 1153–1164. https://doi.org/10.1111/1365-2745.12437

Olson, R.J., Zettler, E.R., Anderson, O.K., 1989. Discrimination of eukaryotic phytoplankton cell types from light scatter and autofluorescence properties measured by flow cytometry. Cytometry 10, 636–643. https://doi.org/10.1002/cyto.990100520

Otero, J., Álvarez-Salgado, X.A., Bode, A., 2020. Phytoplankton Diversity Effect on Ecosystem Functioning in a Coastal Upwelling System. Front. Mar. Sci. 7:592255. https://doi.org/10.3389/fmars.2020.592255

Paczkowska, J., Rowe, O.F., Figueroa, D., Andersson, A., 2019. Drivers of phytoplankton production and community structure in nutrient-poor estuaries receiving terrestrial organic inflow. Mar. Environ. Res. 151, 104778. https://doi.org/10.1016/j.marenvres.2019.104778

Pandey, U., Pandey, J., 2015. The Skewed N:P Stoichiometry Resulting from Anthropogenic Drivers Regulate Production of Transparent Exopolymer Particles (TEP) in Ganga River. Bull. Environ. Contam. Toxicol. 94, 118–124. https://doi.org/10.1007/s00128-014-1344-0

Parinos, C., Gogou, A., Krasakopoulou, E., Lagaria, A., Giannakourou, A., Karageorgis, A.P., Psarra, S., 2017. Transparent Exopolymer Particles (TEP) in the NE Aegean Sea frontal area: Seasonal dynamics under the influence of Black Sea water. Cont. Shelf Res., Investigating fertilizing mechanisms and ecosystem functioning in an E. Mediterranean productivity "hotspot": The case of the oligotrophic NE Aegean Sea 149, 112–123. https://doi.org/10.1016/j.csr.2017.03.012

Park, M.G., Cooney, S.K., Yih, W., Coats, D.W., 2002. Effects of two strains of the parasitic dinoflagellate *Amoebophrya* on growth, photosynthesis, light absorption, and quantum yield of bloom-forming dinoflagellates. Mar. Ecol. Prog. Ser. 227, 281–292. https://doi.org/10.3354/meps227281

Passow, U., Alldredge, A.L., 1996. A dye-binding assay for the spectrophotometric measurement of transparent exopolymer particles (TEP). Oceanogr. Lit. Rev. 7, 669.

Piehler, M.F., Twomey, L.J., Hall, N.S., Paerl, H.W., 2004. Impacts of inorganic nutrient enrichment on phytoplankton community structure and function in Pamlico Sound, NC, USA. Estuar. Coast. Shelf Sci. 61, 197–209. https://doi.org/10.1016/j.ecss.2004.05.001

Probyn, T.A., Painting, S.J., 1985. Nitrogen uptake by size-fractionated phytoplankton populations in Antarctic surface waters1. Limnol. Oceanogr. 30, 1327–1332. https://doi.org/10.4319/lo.1985.30.6.1327
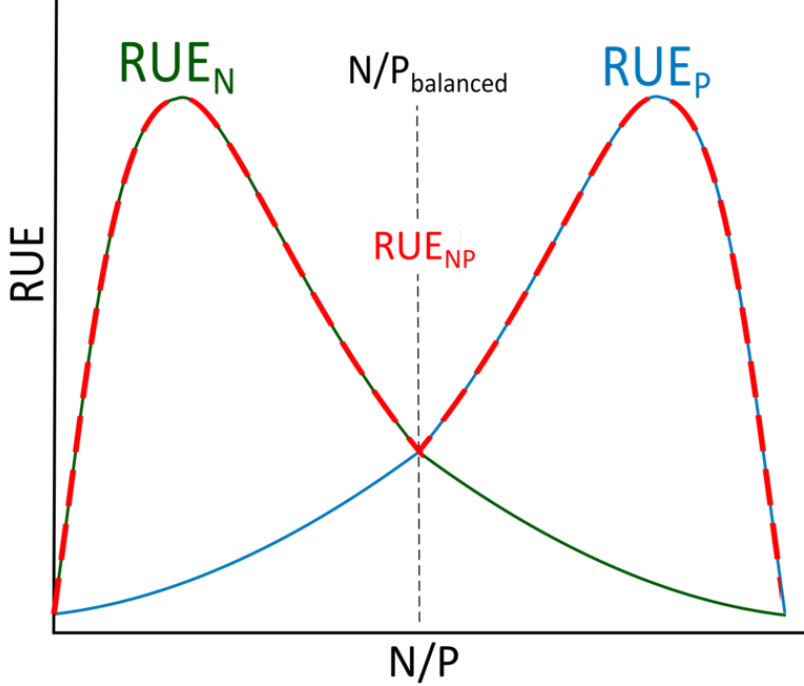
Ptacnik, R., Andersen, T., Tamminen, T., 2010. Performance of the Redfield Ratio and a Family of Nutrient Limitation Indicators as Thresholds for Phytoplankton N vs. P Limitation. Ecosystems 13, 1201–1214. https://doi.org/10.1007/s10021-010-9380-z
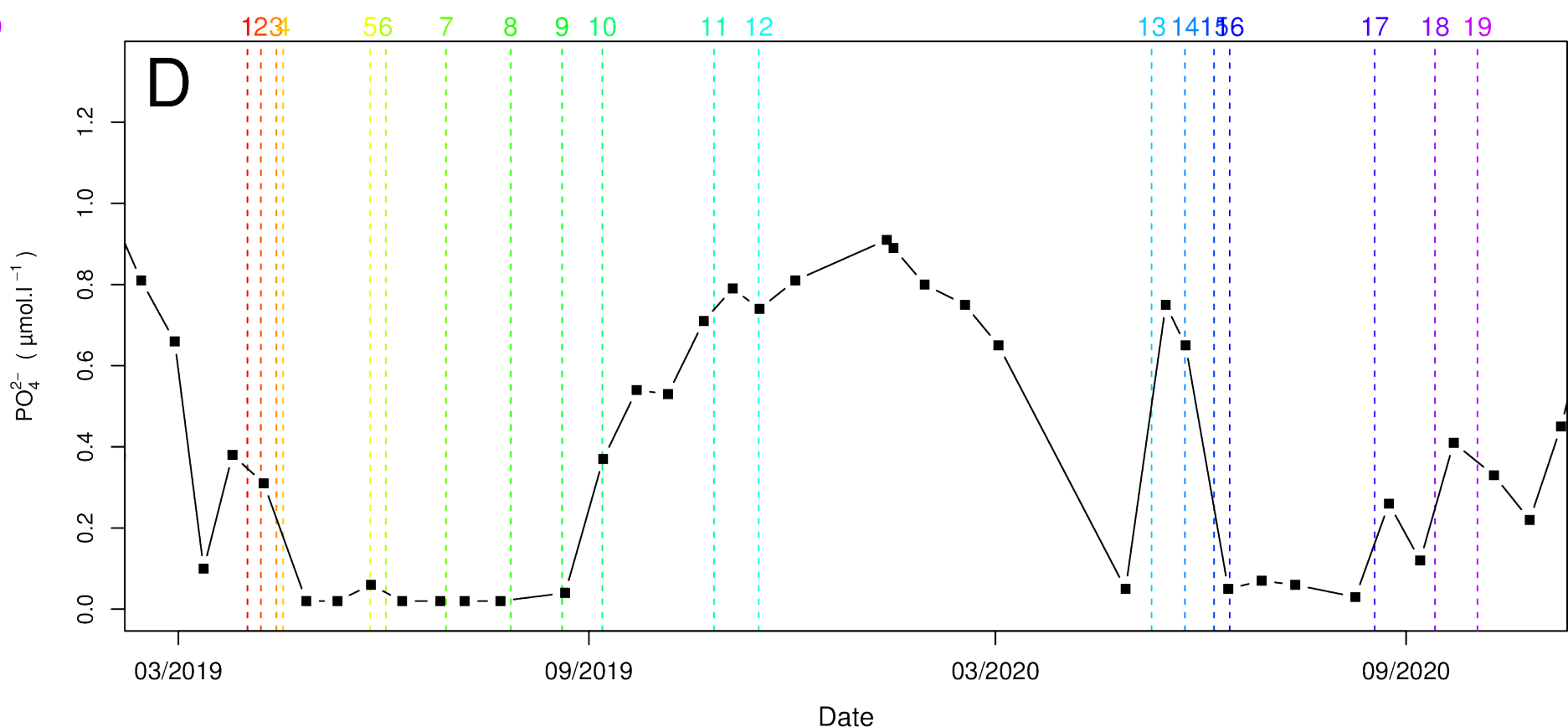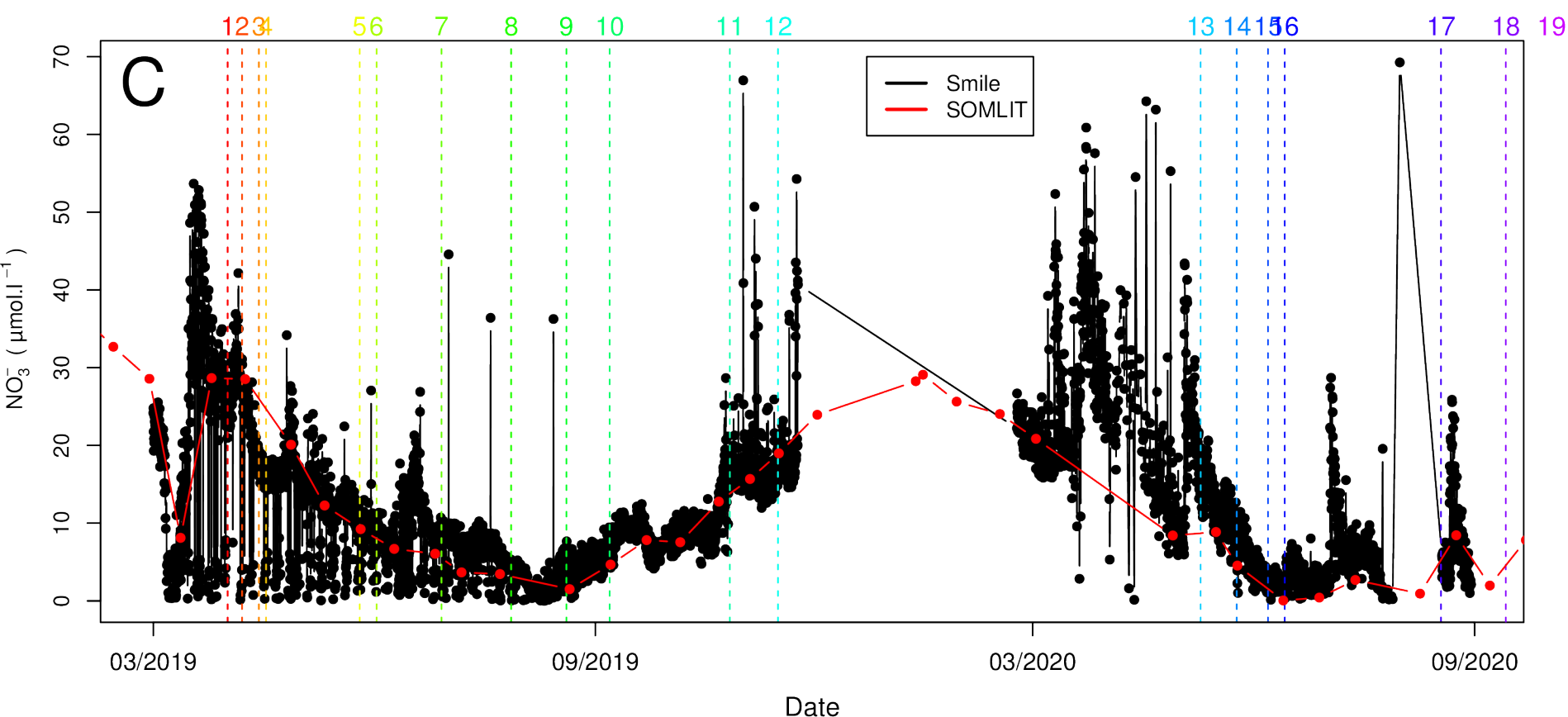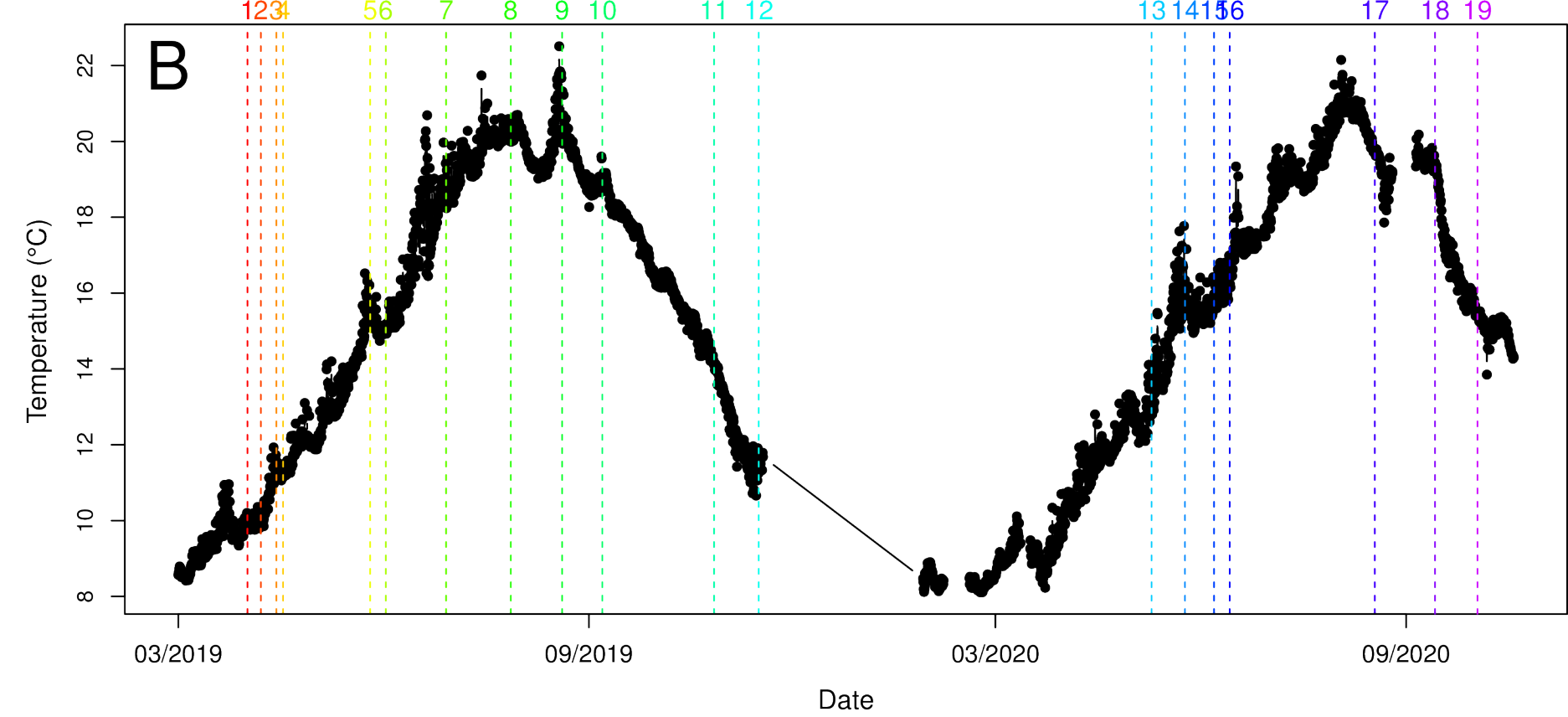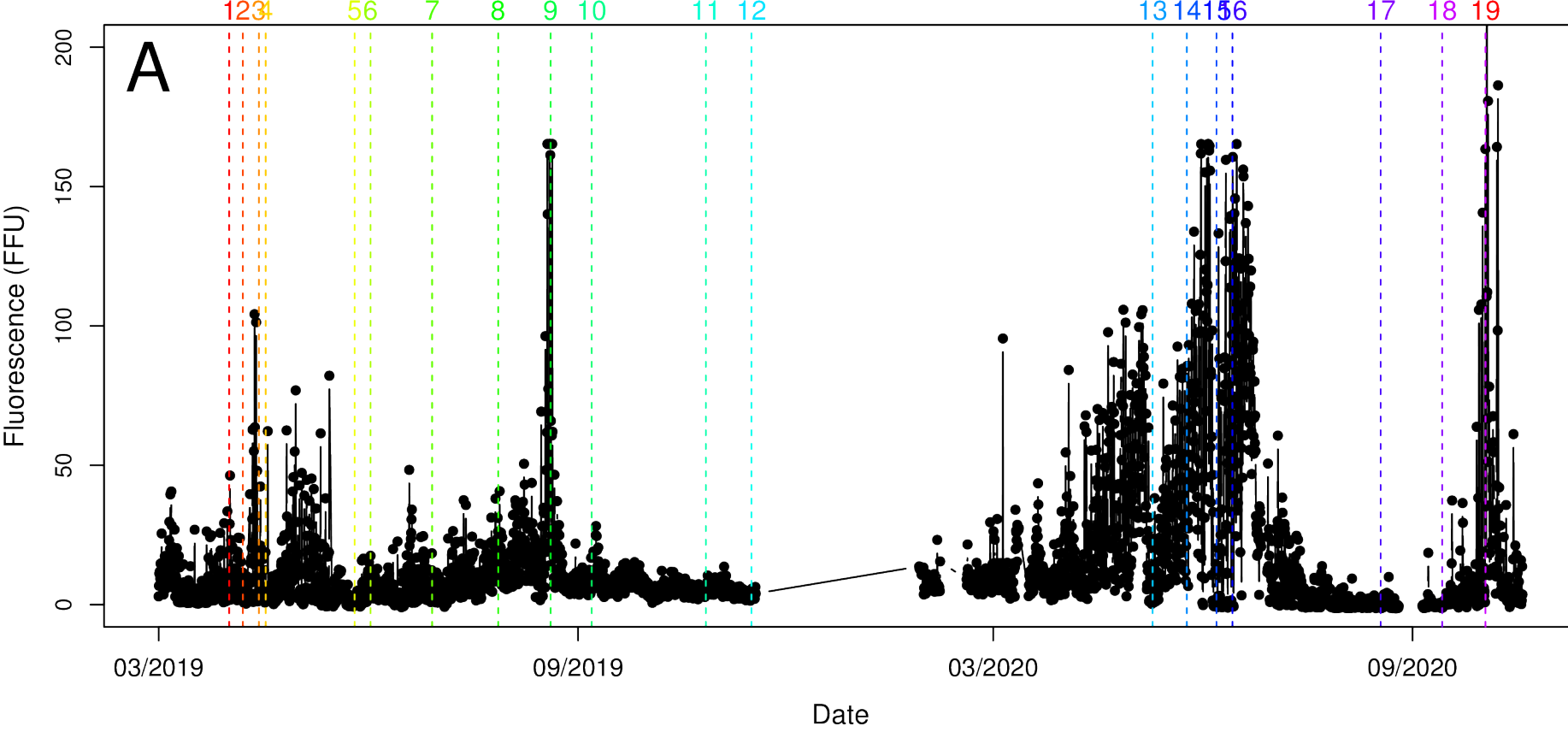
Ptacnik, R., Solimini, A.G., Andersen, T., Tamminen, T., Brettum, P., Lepistö, L., Willén, E., Rekolainen, S., 2008. Diversity predicts stability and resource use efficiency in natural phytoplankton communities. Proc. Natl. Acad. Sci. 105, 5134–5138. https://doi.org/10.1073/pnas.0708328105
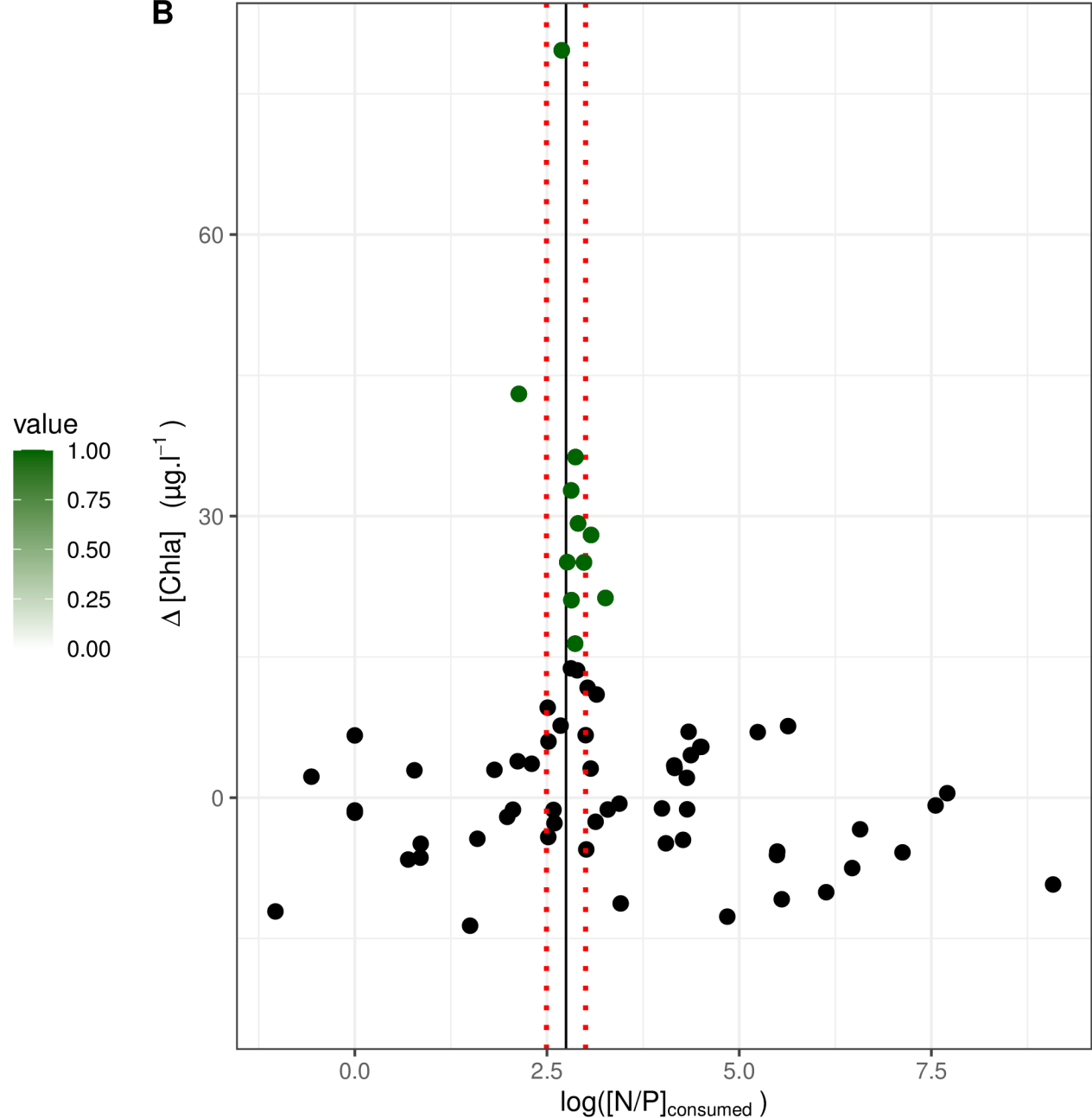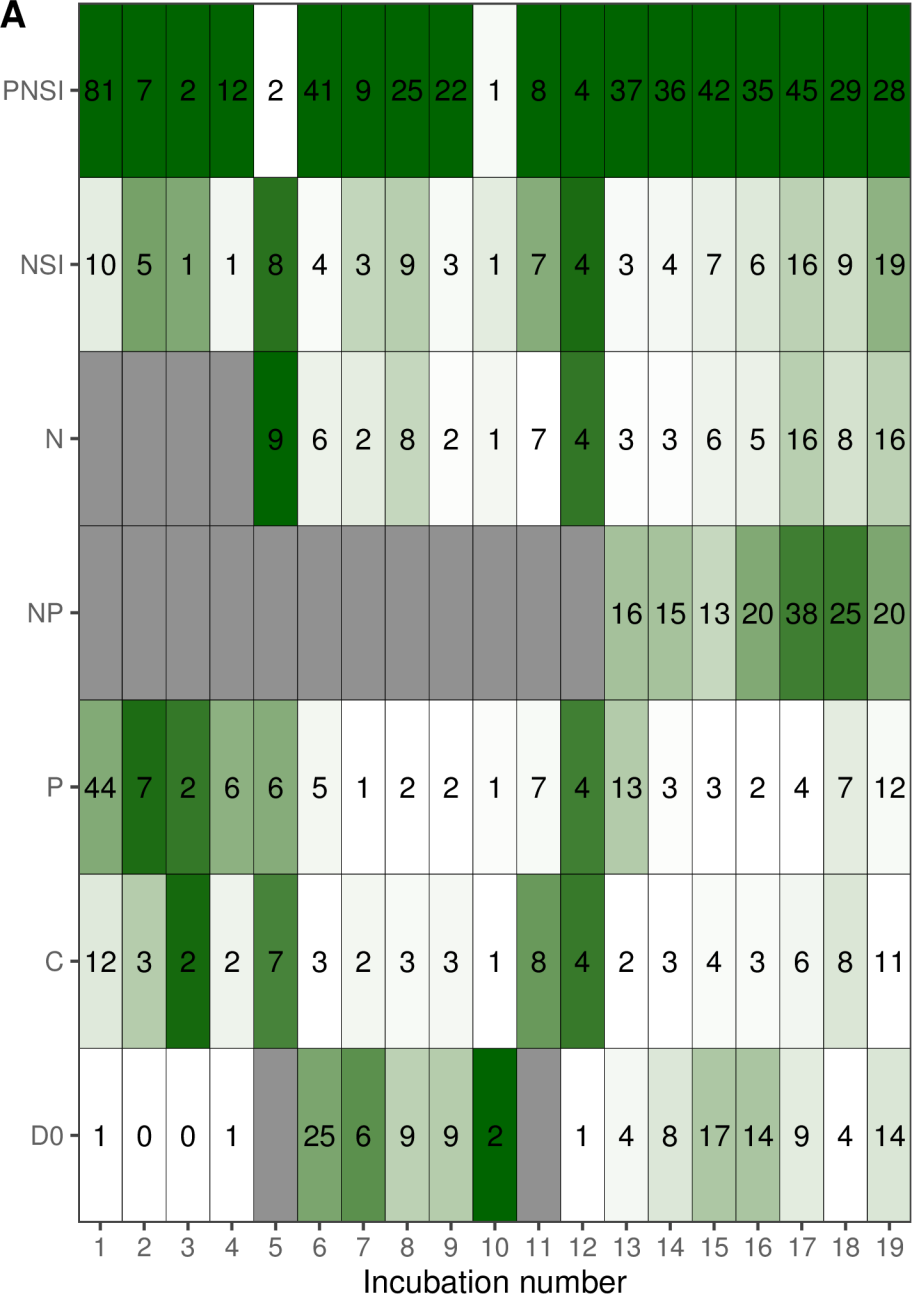
Rabalais, N.N., Turner, R.E., Díaz, R.J., Justić, D., 2009. Global change and eutrophication of coastal waters. ICES J. Mar. Sci. 66, 1528–1537. https://doi.org/10.1093/icesjms/fsp047
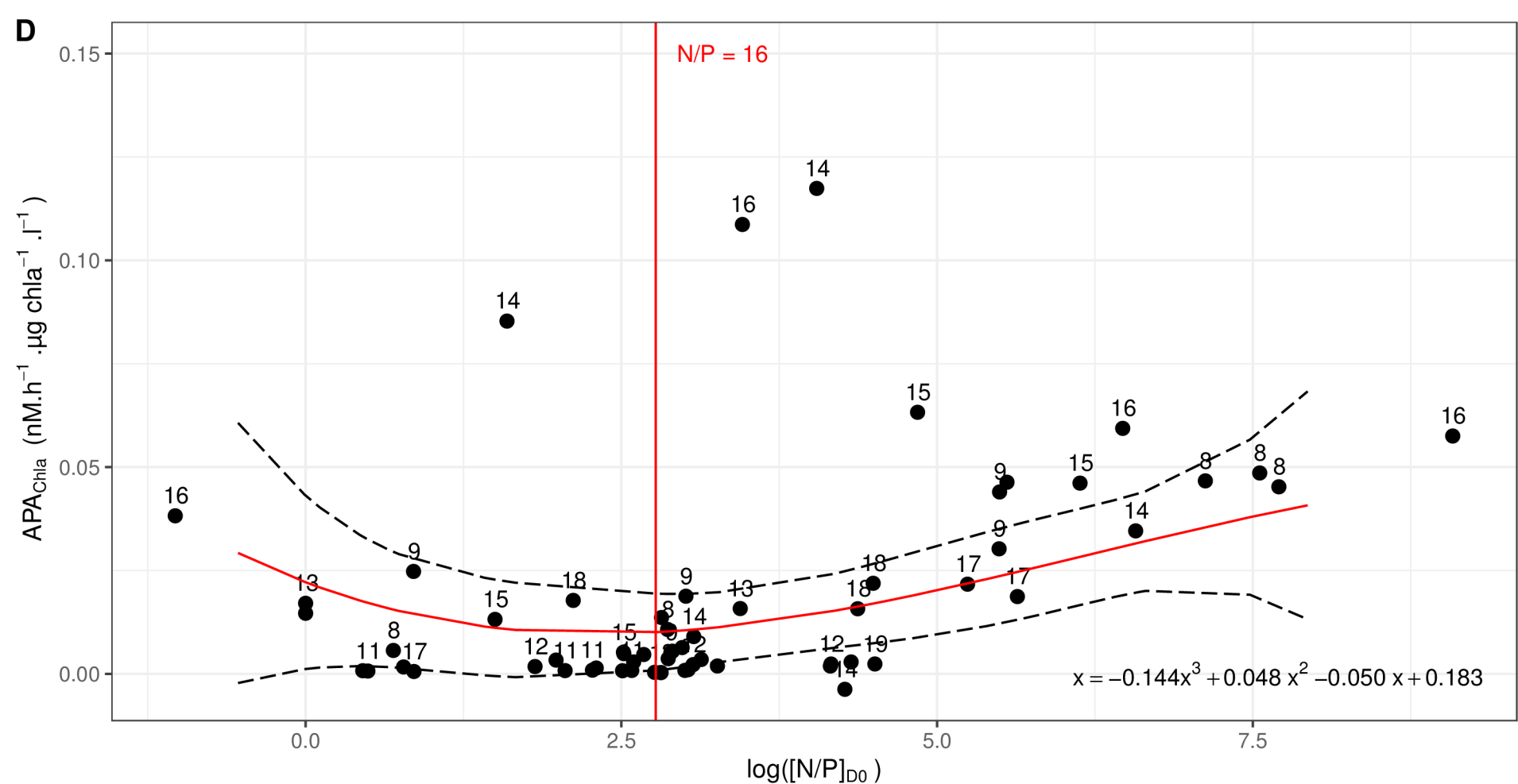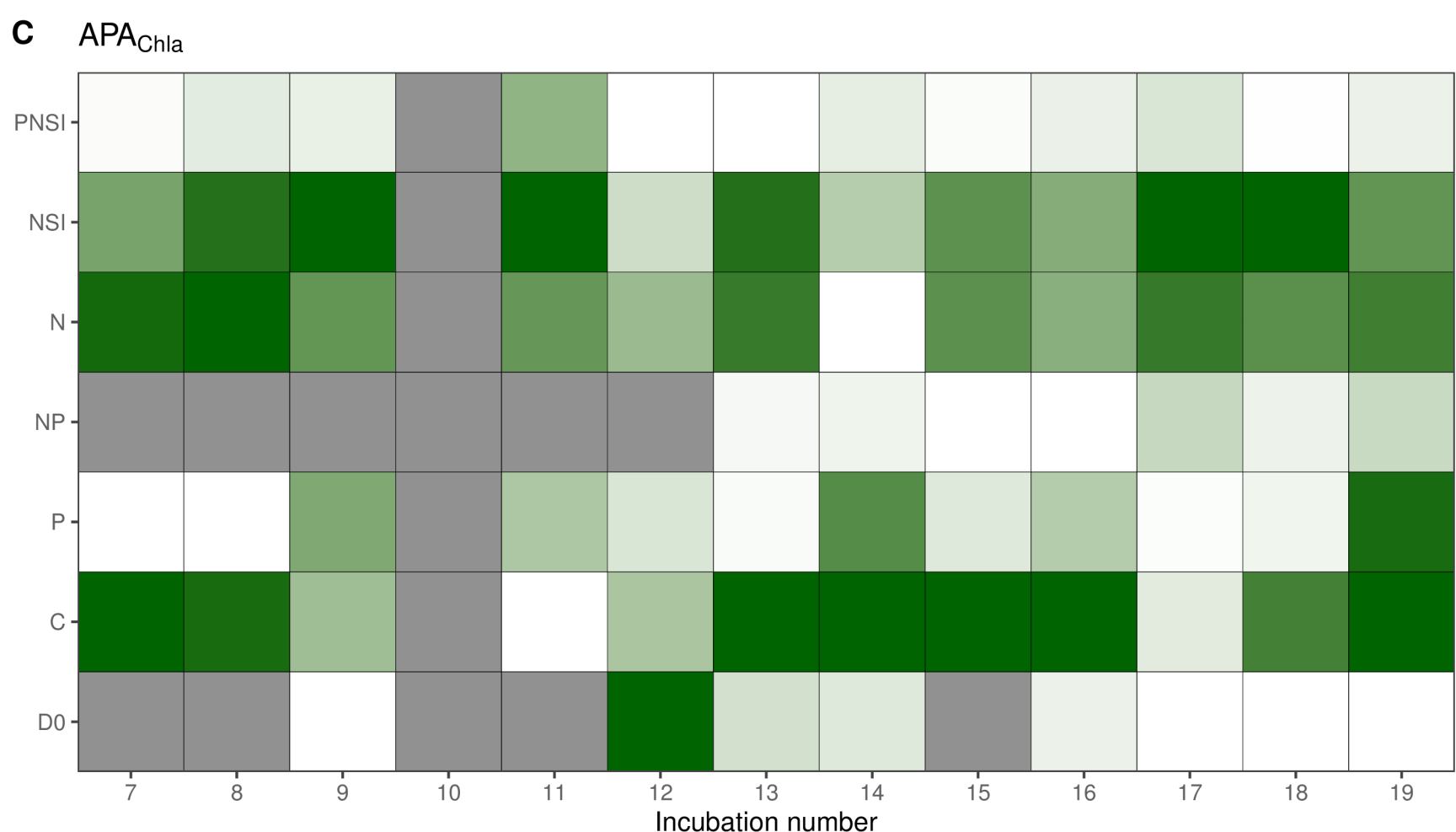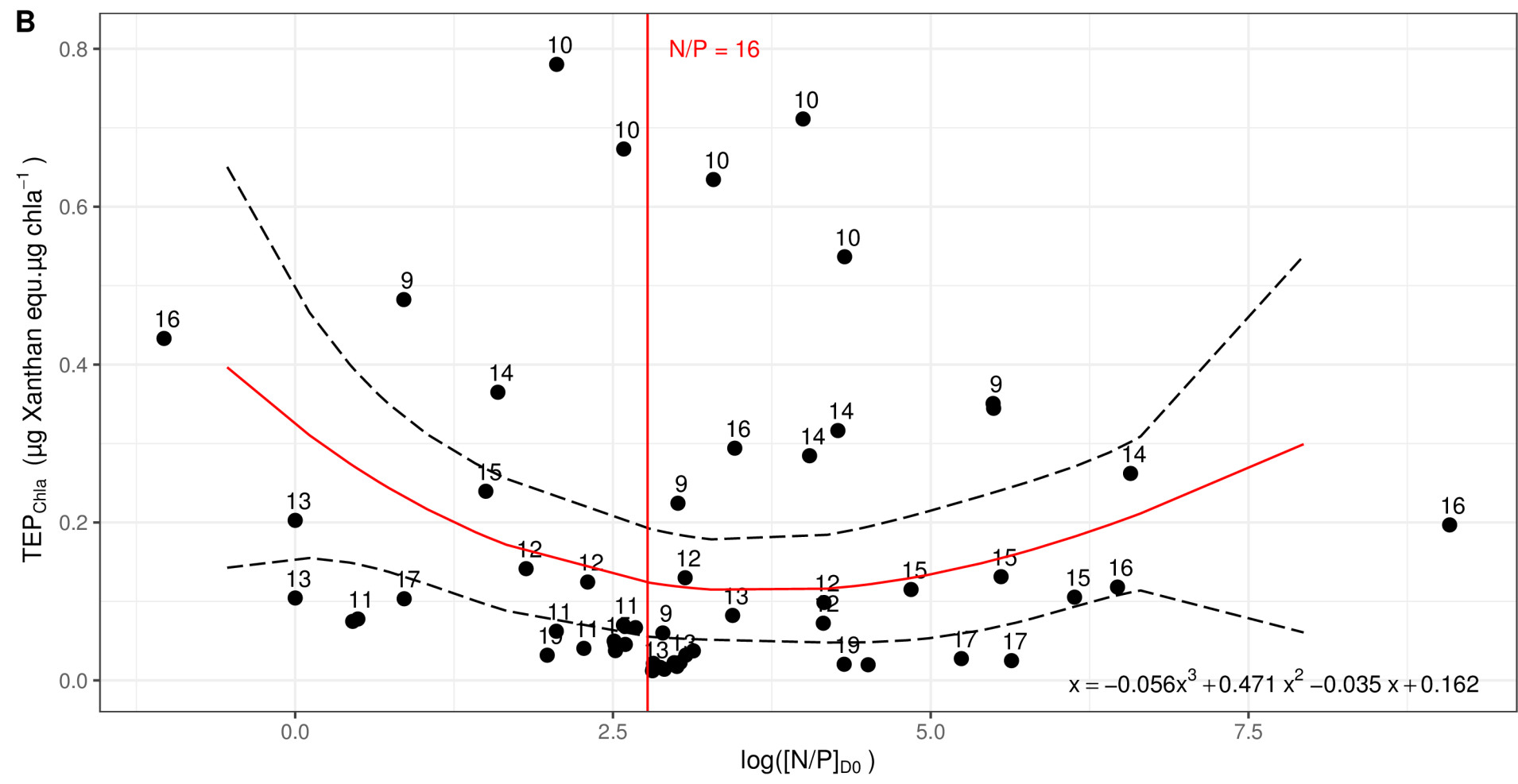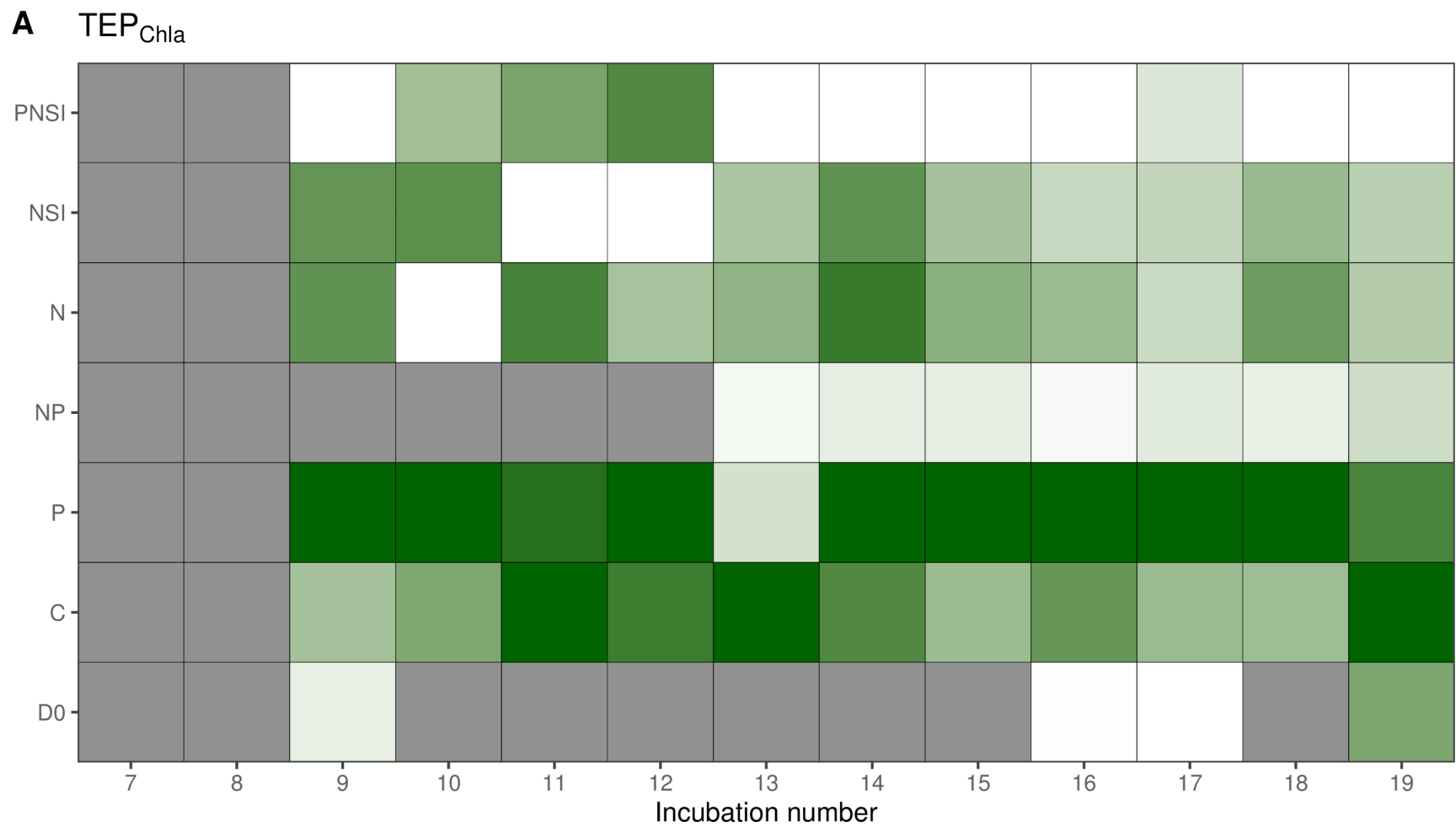
757 Rahav, E., Raveh, O., Hazan, O., Gordon, N., Kress, N., Silverman, J., Herut, B., 2018.
758   Impact of nutrient enrichment on productivity of coastal water along the SE
759   Mediterranean shore of Israel - A bioassay approach. Mar. Pollut. Bull. 127, 559–567.
760   https://doi.org/10.1016/j.marpolbul.2017.12.048

761 Redfield, A.C., 1958. The biological control of chemical factors in the environment. Am. Sci.
762   46, 230A–221.

763 Reed, M.L., Pinckney, J.L., Keppler, C.J., Brock, L.M., Hogan, S.B., Greenfield, D.I., 2016.
764   The influence of nitrogen and phosphorus on phytoplankton growth and assemblage
765   composition in four coastal, southeastern USA systems. Estuar. Coast. Shelf Sci. 177,
766   71–82. https://doi.org/10.1016/j.ecss.2016.05.002

767 Saito, M.A., Goepfert, T.J., Ritt, J.T., 2008. Some thoughts on the concept of colimitation:
768   Three definitions and the importance of bioavailability. Limnol. Oceanogr. 53, 276–
769   290. https://doi.org/10.4319/lo.2008.53.1.0276

770 Serre-Fredj, L., Jacqueline, F., Navon, M., Izabel, G., Chasselin, L., Jolly, O., Repecaud, M.,
771   Claquin, P., 2021. Coupling high frequency monitoring and bioassay experiments to
772   investigate a harmful algal bloom in the Bay of Seine (French-English Channel). Mar.
773   Pollut. Bull. 168, 112387. https://doi.org/10.1016/j.marpolbul.2021.112387

774 Shen, A., Ishizaka, J., Yang, M., Ouyang, L., Yin, Y., Ma, Z., 2019. Changes in community
775   structure and photosynthetic activities of total phytoplankton species during the
776   growth, maintenance, and dissipation phases of a *Prorocentrum donghaiense* bloom.
777   Harmful Algae 82, 35–43. https://doi.org/10.1016/j.hal.2018.12.007

778 Song, X., Tan, M., Xu, G., Su, X., Liu, J., Ni, G., Li, Y., Tan, Y., Huang, L., Shen, P., Li, G.,
779   2019. Is phosphorus a limiting factor to regulate the growth of phytoplankton in Daya
780   Bay, northern South China Sea: a mesocosm experiment. Ecotoxicology 28, 559–568.
781   https://doi.org/10.1007/s10646-019-02049-7

782 Strickland, J.D.H., Parsons, T.R., 1972. A Practical Handbook of Seawater Analysis. Bull.
783   Fish. Res. Board Can. 310.

784 Tamminen, T., Andersen, T., 2007. Seasonal phytoplankton nutrient limitation patterns as
785   revealed by bioassays over Baltic Sea gradients of salinity and eutrophication. Mar.
786   Ecol. Prog. Ser. 340, 121–138. https://doi.org/10.3354/meps340121

787 Tanaka, T., Henriksen, P., Lignell, R., Olli, K., Seppälä, J., Tamminen, T., Thingstad, T.F.,
788   2006. Specific Affinity for Phosphate Uptake and Specific Alkaline Phosphatase
789   Activity as Diagnostic Tools for Detecting Phosphorus-Limited Phytoplankton and
790   Bacteria. Estuaries Coasts 29, 1226–1241.

791 Thyssen, M., Grégori, G.J., Grisoni, J.-M., Pedrotti, M.L., Mousseau, L., Artigas, L.F., Marro,
792   S., Garcia, N., Passafiume, O., Denis, M.J., 2014. Onset of the spring bloom in the
793   northwestern Mediterranean Sea: influence of environmental pulse events on the in
794   situ hourly-scale dynamics of the phytoplankton community structure. Front.
795   Microbiol. 5:387. https://doi.org/10.3389/fmicb.2014.00387

796 Van Meerssche, E., Pinckney, J.L., 2019. Nutrient Loading Impacts on Estuarine
797   Phytoplankton Size and Community Composition: Community-Based Indicators of
798   Eutrophication. Estuaries Coasts 42, 504–512. https://doi.org/10.1007/s12237-018-
799   0470-z

800 Watanabe, K., Kasai, A., Fukuzaki, K., Ueno, M., Yamashita, Y., 2017. Estuarine circulation-
801   driven entrainment of oceanic nutrients fuels coastal phytoplankton in an open coastal
802   system in Japan. Estuar. Coast. Shelf Sci. 184, 126–137.
803   https://doi.org/10.1016/j.ecss.2016.10.031

804 Xu, H., Paerl, H.W., Qin, B., Zhu, G., Gaoa, G., 2010. Nitrogen and phosphorus inputs control
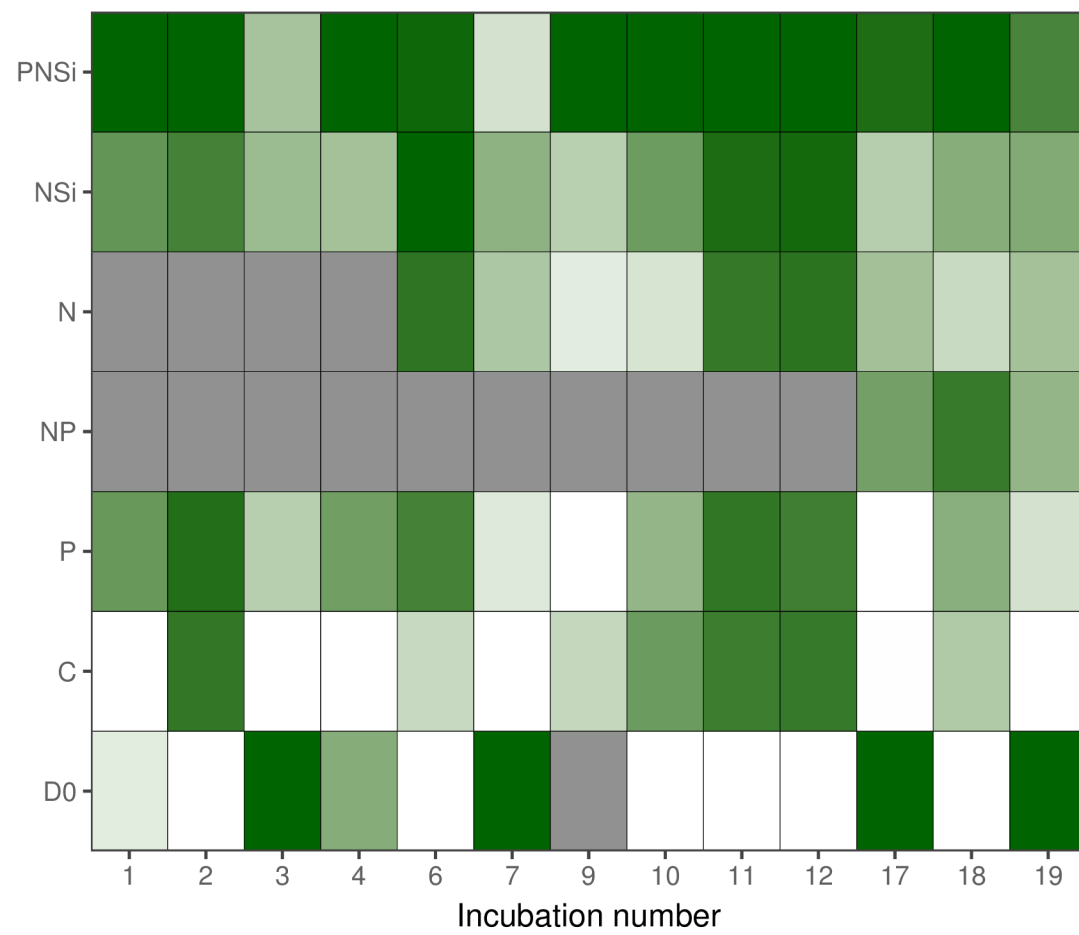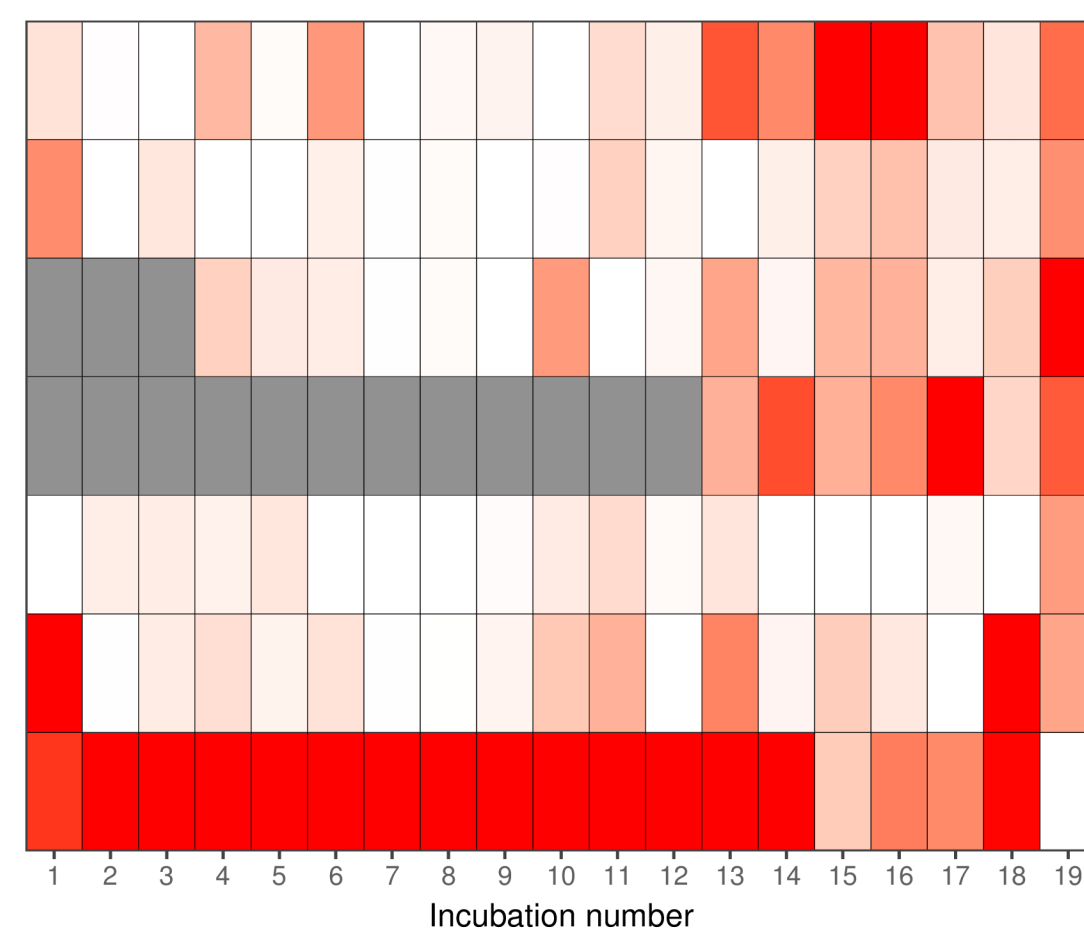805   phytoplankton growth in eutrophic Lake Taihu, China. Limnol. Oceanogr. 55, 420–
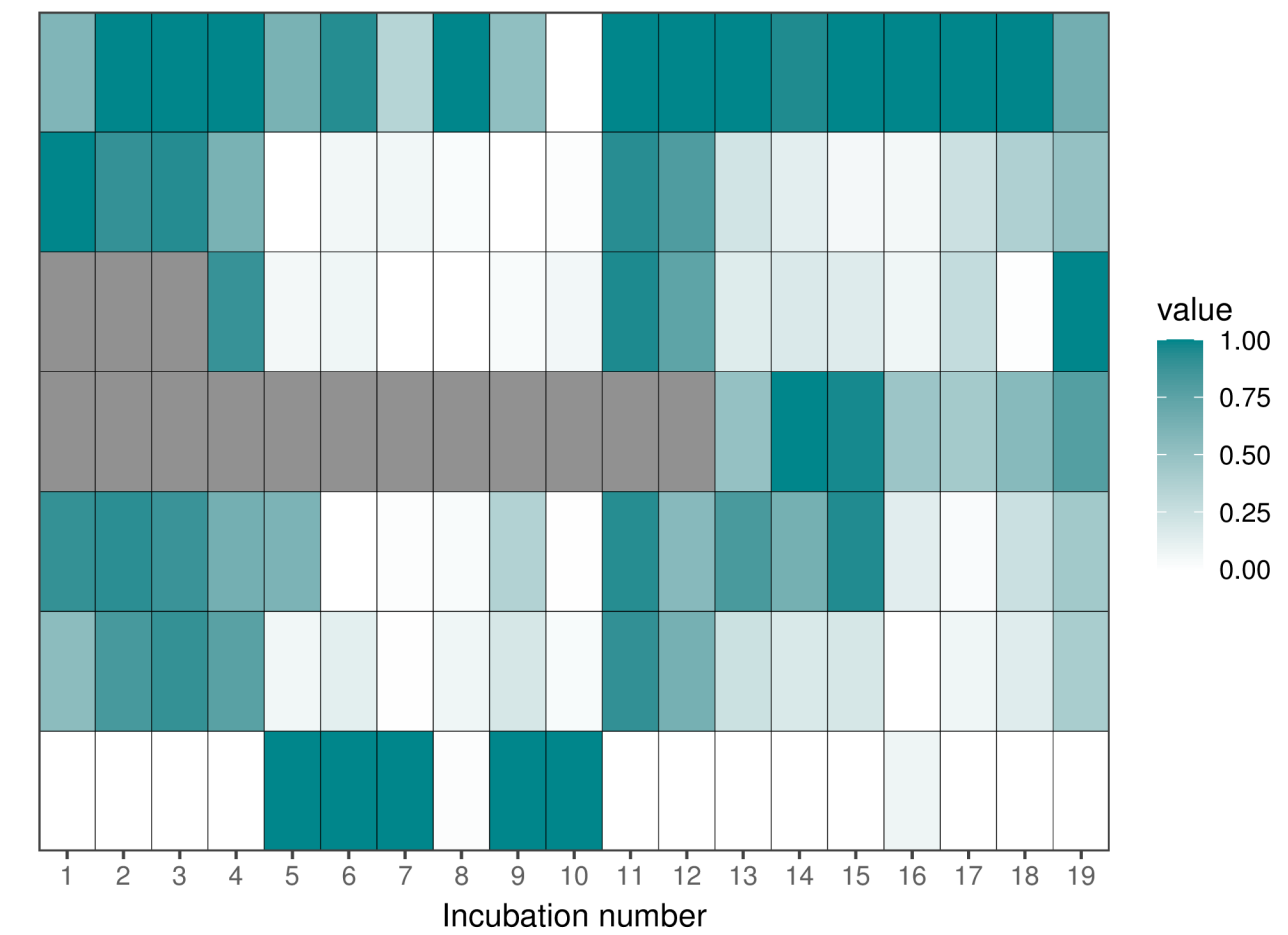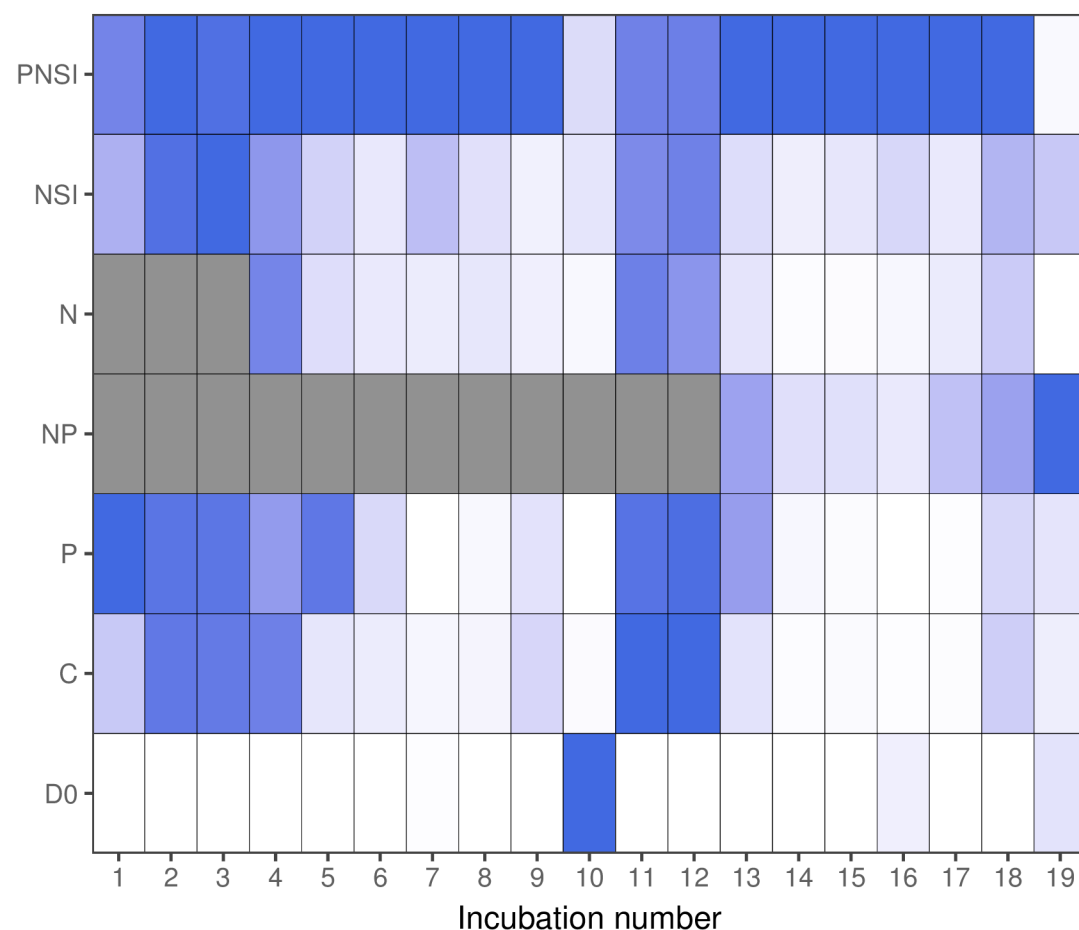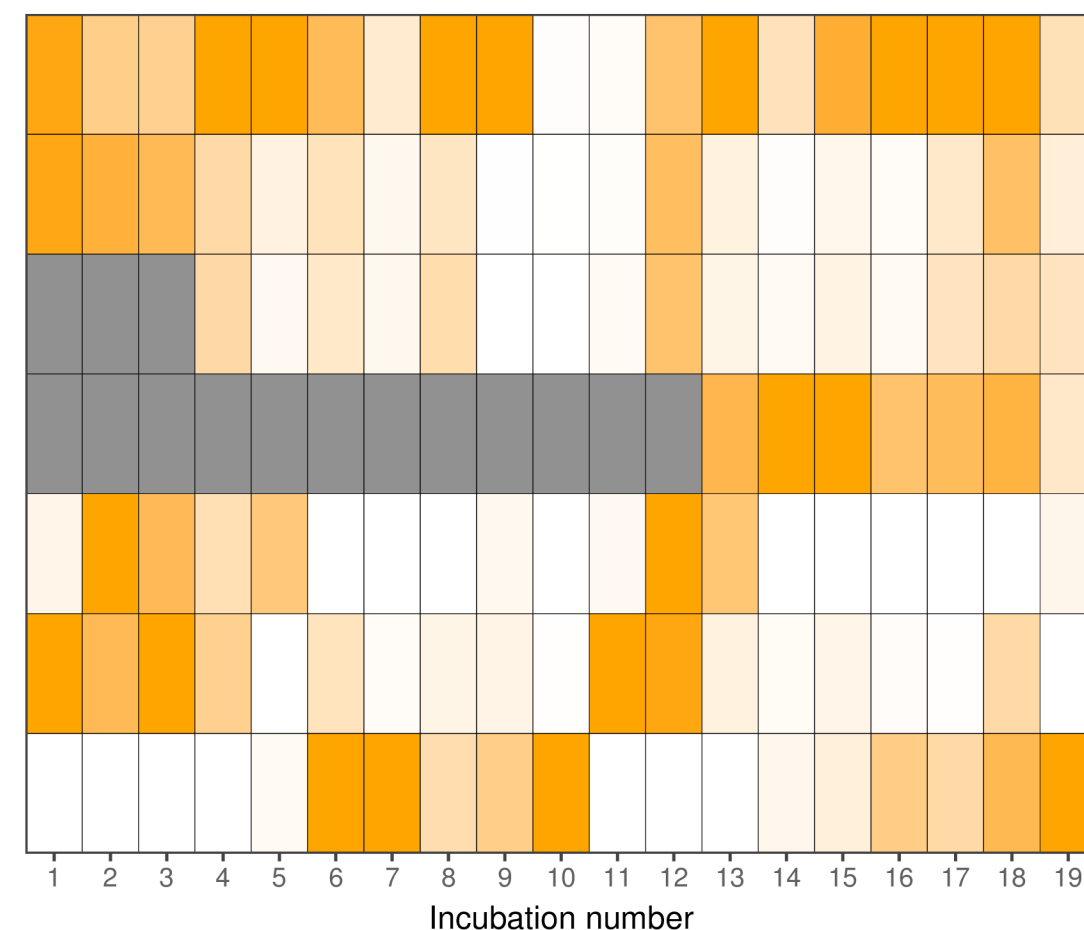806   432. https://doi.org/10.4319/lo.2010.55.1.0420

807   Yang, J.R., Yu, X., Chen, H., Kuo, Y.-M., Yang, J., 2021. Structural and functional variations
808   of phytoplankton communities in the face of multiple disturbances. J. Environ. Sci.
809   100, 287–297. https://doi.org/10.1016/j.jes.2020.07.026
810   Yuan, Y., Bi, Y., Hu, Z., 2017. Phytoplankton communities determine the spatio-temporal
811   heterogeneity of alkaline phosphatase activity: evidence from a tributary of the Three
812   Gorges Reservoir. Sci. Rep. 7, 16404. https://doi.org/10.1038/s41598-017-16740-4
813   Zaoli, S., Giometto, A., Marañón, E., Escrig, S., Meibom, A., Ahluwalia, A., Stocker, R.,
814   Maritan, A., Rinaldo, A., 2019. Generalized size scaling of metabolic rates based on
815   single-cell measurements with freshwater phytoplankton. Proc. Natl. Acad. Sci. 116,
816   17323–17329. https://doi.org/10.1073/pnas.1906762116
817   Zhang, M., Yu, Y., Yang, Z., Kong, F., 2012. Photochemical responses of phytoplankton to
818   rapid increasing-temperature process. Phycol. Res. 60, 199–207.
819   https://doi.org/10.1111/j.1440-1835.2012.00654.x
820   Zheng, L., Zhai, W., Wang, L., Huang, T., 2020. Improving the understanding of central Bohai
821   Sea eutrophication based on wintertime dissolved inorganic nutrient budgets: Roles of
822   north Yellow Sea water intrusion and atmospheric nitrogen deposition. Environ.
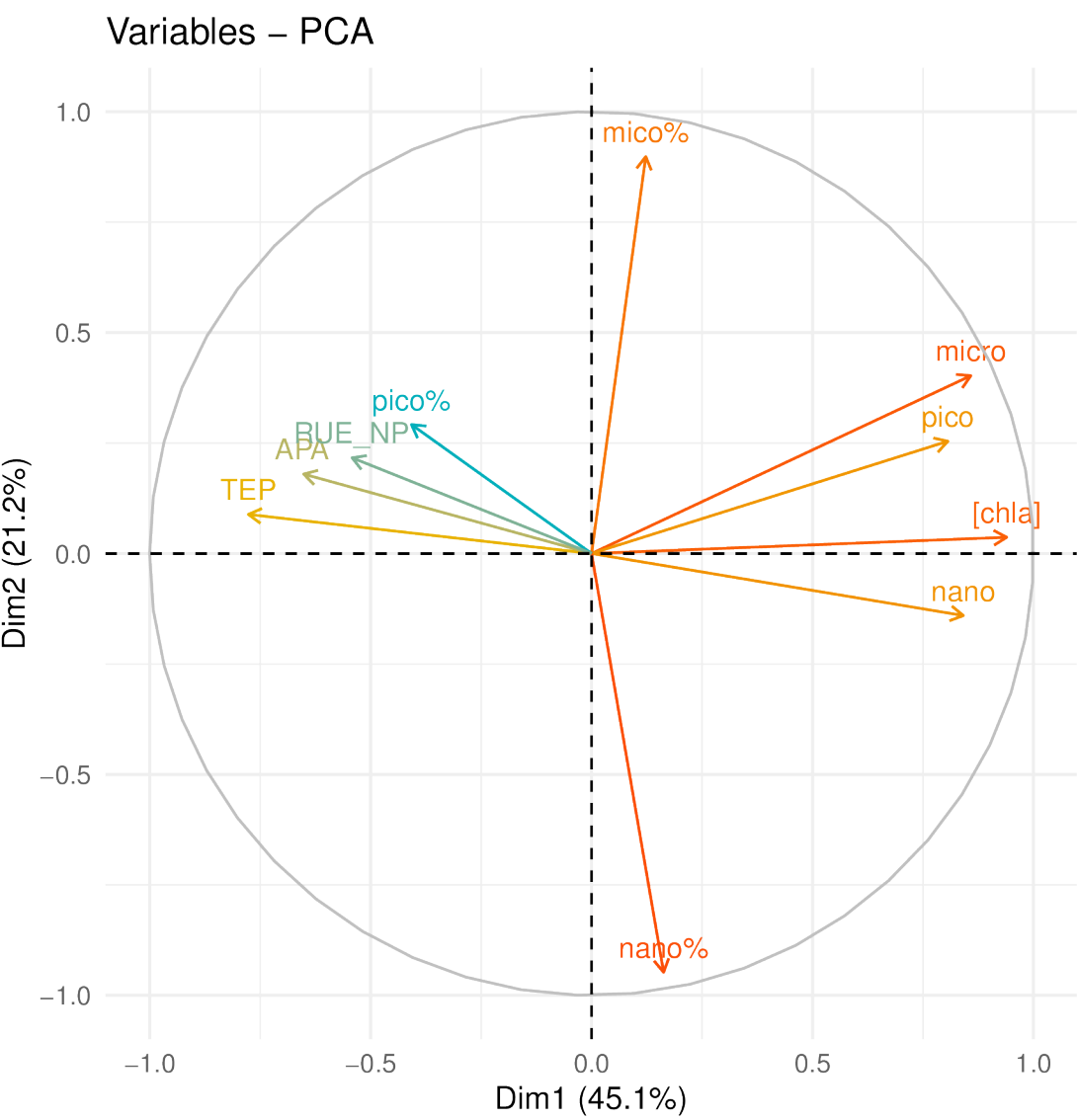823   Pollut. 267, 115626. https://doi.org/10.1016/j.envpol.2020.115626
824

A

	1	2	3	4	5	6	7	8	9	10	11	12	13	14	15	16	17	18	19
PNSI	81	7	2	12	2	41	9	25	22	1	8	4	37	36	42	35	45	29	28
NSI	10	5	1	1	8	4	3	9	3	1	7	4	3	4	7	6	16	9	19
N					9	6	2	8	2	1	7	4	3	3	6	5	16	8	16
NP													16	15	13	20	38	25	20
P	44	7	2	6	6	5	1	2	2	1	7	4	13	3	3	2	4	7	12
C	12	3	2	2	7	3	2	3	3	1	8	4	2	3	4	3	6	8	11
D0	1	0	0	1		25	6	9	9	2		1	4	8	17	14	9	4	14

Incubation number

B

A TEP$_{Chla}$

B
$$x = -0.056x^3 + 0.471x^2 - 0.035x + 0.162$$

C APA$_{Chla}$

D
$$x = -0.144x^3 + 0.048x^2 - 0.050x + 0.183$$

A FvFm   B *Synechoccocus*   C Picoeukaryotes   D Nanoeukaryotes   E Cryptophyte   F Microphytoplankton
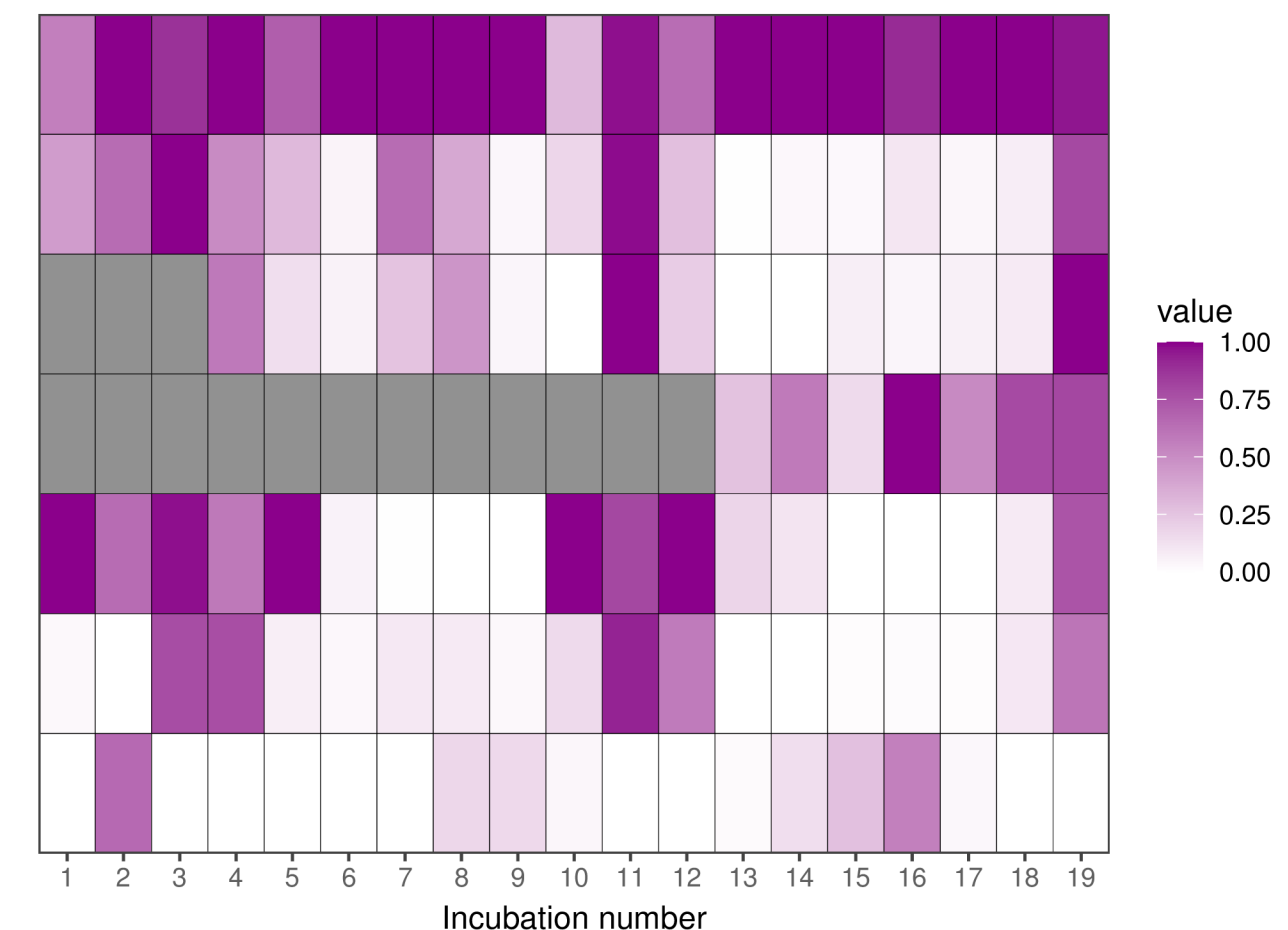
A Variables – PCA

B Cluster plot

C Cluster Dendrogram